Journal of Cleaner Production 434 (2024) 139782

Contents lists available at ScienceDirect

Journal of Cleaner Production

journal homepage: www.elsevier.com/locate/jclepro

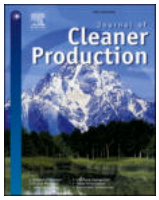

# Comparative energy performance analysis of micro gas turbine and internal combustion engine in a cogeneration plant based on biomass gasification

Mariaconcetta Fatiguso, Alessandro R. Valenti, Silvia Ravelli *

*Department of Engineering and Applied Sciences, University of Bergamo, 24044 Dalmine, Italy*

ARTICLE INFO

Handling Editor: Santanu Bandyopadhyay

*Keywords:*
Biomass
Gasification
Internal combustion engine
Micro gas turbine
Part load
Load-following

ABSTRACT

With a view to replacing fossil fuels, biomass electricity generation worldwide has grown from 509 TWh in 2015 to 685 TWh in 2021 and an upward trend is expected for the next years. It is about dispatchable, low-emission power to complement generation from variable renewables. Although modern bioenergy is considered a stable and carbon-neutral source, there is a need to boost the efficiency of the Biomass-to-Energy (BtE) conversion technologies. Accordingly, in this modeling study, attention was drawn to biomass gasification for heat and power, with a special focus on the prime mover characterization for distributed generation. An internal combustion engine (ICE) and a micro gas turbine (mGT), having the same nominal capacity of about 240 $kW_{el}$ when fueled by natural gas (NG), were inserted into a two-way biomass gasification chain and hence fed by clean syngas deriving from a downdraft gasifier. Simulations of the main components of the thermal power plant (gasifier, syngas cleanup, power island) were validated against data available in the published literature and in technical sheets, for specific operating conditions. The next step was to evaluate the overall performance of the entire BtE chain in terms of electrical, thermal, and total efficiency, both at full and part load, in order to highlight the pros and cons of each generator, in a twofold perspective. The last goal was to simulate a load following strategy, for two typical cold and hot days. The results of the thermodynamic analysis indicate that ICE is better performing than mGT, in the simulated context where the power demand from the grid ranges from 80 $kW_{el}$ to 190 $kW_{el}$, with an ambient temperature between 2 and 35 °C. ICE provides the best performance in CHP mode, with a total efficiency of 62–69%.

## 1. Introduction

Since the turn of the century, biopower generation has seen an increasing trend, with solid biomass playing the main role, followed by biogas and municipal waste. Bioenergy for electricity generation is expected to nearly double, from 750 TWh in 2021 to about 1350 TWh in 2030 (IEA, 2022), in order to pursue carbon neutrality and energy diversification while balancing variable renewables such as wind and solar. On the one hand, high flexibility in reducing emissions and replacing fossil fuels can be attained in different contexts, since almost every country can exploit its own local biomass resource. On the other hand, sustainability issues related to competition for land use and loss of biodiversity may limit its use.

### 1.1. Regulatory background

In the Net Zero Scenario there are no plans to expand cultivated land for bioenergy or to convert existing forest land to bioenergy crops, so waste and biomass residues will be used. Moreover, efficient utilization is highly recommended, at least in the European Union (EU), where the new Renewable Energy Directive 2018/2001 (RED II) introduced sustainability and greenhouse gas emissions saving criteria for biomass fuels used in the electricity sector, heating cooling, compared with the previous renewable energy sources directive 2009/28/EC (Squilbin et al., 2020). New installations for electricity production from biomass fuels, with a thermal input over 50 MW, must comply with the following:

- for a rated thermal power input ($P_{th,i}$) from 50 to 100 MW, high-efficiency cogeneration technology is required or, for electricity-only, the best available techniques should be applied;
- for a rated $P_{th,i}$ over 100 MW, high-efficiency cogeneration technology is again needed or, for electricity-only, a net electrical efficiency ($\eta_{el,n}$) of at least 36% should be achieved.

Furthermore, the greenhouse gas emission savings from the use of

* Corresponding author. Department of Engineering and Applied Sciences, University of Bergamo, Marconi St. 5, 24044 Dalmine, Italy.
*E-mail address:* silvia.ravelli@unibg.it (S. Ravelli).

https://doi.org/10.1016/j.jclepro.2023.139782
Received 30 July 2023; Received in revised form 18 October 2023; Accepted 14 November 2023
Available online 20 November 2023

**Nomenclature**

| | |
|---|---|
| A | heat exchange area |
| A/F | air-fuel ratio |
| BtE | Biomass-to-Energy |
| C | dimensional constant |
| CCE | carbon conversion efficiency |
| CF | compressor corrected flow |
| CGE | cold gas efficiency |
| CHP | combined heat and power |
| CS | corrected speed |
| EU | European Union |
| FC | fuel compressor |
| FF | turbine inlet flow function |
| h | enthalpy |
| HHV | higher heating value |
| HT | high temperature |
| ICE | internal combustion engine |
| LHV | lower heating value |
| LT | low temperature |
| m | mass flow rate |
| mGT | micro gas turbine |
| MW | molecular weight |
| n | rotational speed |
| NG | natural gas |
| P | power |
| p | pressure |
| pp | percentage points |
| R | gas constant |
| SGE | Siemens gas engine |
| T | temperature |
| TIT | turbine inlet temperature |
| TOT | turbine outlet temperature |
| U | heat transfer coefficient |
| β | pressure ratio |
| γ | ratio of specific heat |
| ε | effectiveness |
| η | efficiency |

*Subscript*

| | |
|---|---|
| a | air |
| amb | ambient |
| aux | auxiliary |
| C | compressor |
| D | design |
| el | electrical |
| exh | exhaust |
| FC | fuel compressor |
| fuel | fuel input |
| g | gross |
| i | input |
| in | inlet |
| is | isentropic |
| n | net |
| out | outlet |
| pe | power electronics |
| ref | reference |
| T | turbine |
| th | thermal |
| tot | total |
| y | polytropic |

*Superscript*

| | |
|---|---|
| b | biomass |
| s | syngas |

biomass fuels shall be at least 70% or 80% for electricity generation in installations that start operation after January 1, 2021 or 2026, respectively. Note that these EU criteria apply to electricity, heating and cooling production provided that the total $P_{th,i}$ exceeds 20 MW or 2 MW, in the case of solid or gaseous biomass fuels, respectively (Article 29-RED II). Such a regulatory framework, however complex, is aimed at increasing the efficiency of the BtE processes and improving the level of energy recovery. In fact, stakeholders' concerns include the low conversion efficiency of some BtE applications, as well as insufficient greenhouse gas savings, regardless of the carbon neutrality of biomass (Schipfer, 2019). These issues mainly affect "traditional" use of biomass in older combustion systems or electricity-only plants. It follows that the potential of high-efficient cogeneration should be fully exploited, especially in small and medium installations to promote distributed energy generation while using the heat locally, thus compensating for the lack of district heating infrastructure. In addition, adverse impacts on air quality should be avoided, as incomplete biomass combustion can be an important source of air pollutants that are harmful to human health and the environment.

### 1.2. Goal and scope definition

Consistently with the guidelines above, this study focuses on a small-scale combined heat and power (CHP) system based on biomass gasification, with the goal of pursuing high efficiency and reducing the environmental impact of the BtE pathway. A nominal capacity of about 200 $kW_{el,n}$ was chosen to limit the transport distances of solid biomass, thus lowering supply chain costs and emissions, while avoiding the drawbacks associated with the microscale (La Villetta et al., 2018). Among all thermochemical pathways, gasification was preferred over direct combustion by virtue of greater overall electrical efficiency and flexibility in terms of outputs (electricity, heat, chemicals) and fuel inputs. Additional advantages with respect to full oxidation relate to lower emission of $NO_x$ and $SO_x$, lower reaction temperature, and obviously less requirement of oxygen (Situmorang et al., 2020; Briones-Hidrovo et al., 2021). It is a fact that, in recent years, small-scale woody biomass gasification systems have encountered a noticeable diffusion in Europe, mostly in Germany and in Northern Italy (South Tyrolean region), as documented by Patuzzi et al. (2021). Bocci et al. (2014) confirmed that small biomass gasification plants are a competitive solution to convert waste biomass into syngas for combined heat and power generation, with electrical and cogeneration efficiency of about 20% and 80%, respectively. However, the overall efficiency depends on the "primary conversion" of biomass to a raw gaseous product (syngas) and the "secondary conversion" of clean syngas to heat and energy, with syngas cleanup in between.

### 1.3. Clean syngas production

As for primary conversion, downdraft gasifier is the most suitable for the current purpose, with a capacity between 10 kW and 1 MW, due to its ease of operation and low tar level in the output gas, on condition that the moisture content in the feedstock is below 35% (Susastriawan and Saptoadi, 2017). Thomson et al. (2020) confirmed the predominance of downdraft (fixed-bed) gasifiers among commercial solutions up to 3 $MW_{el}$: syngas is typically characterized by a lower heating value (LHV) of 4–6 $MJ/m^3$ with a tar content of less than 300 $mg/m^3$. Other parameters were reviewed, such as cold gas efficiency (CGE), falling in the

range from 65 to 90%, and carbon conversion efficiency (CCE), less than 85%, provided the fuel moisture content does not exceed 20%. Air is regularly used as gasification medium owing to simplicity of operation (Havilah et al., 2022). For the same reason, atmospheric pressure is recommended for small-scale applications when the purpose is to generate combustible gases (Hamad et al., 2017). The complexity of the thermochemical process of converting a solid biomass to a gaseous fuel has been extensively addressed: production of volatiles and gasification of the char obtained during the devolatilization will occur in stages depending on temperature range, rates of heating, fuel size and porosity (Kirubakaran et al., 2009a). The latter is of particular importance: in highly porous biomass, the large surface area for reactions can ensure uniform composition of the gas produced (Kirubakaran et al., 2009b).

Contaminants from the raw syngas must then be removed: cold gas cleanup relies on relatively mature, high effective techniques pending progress in hot gas cleaning (Woolcock and Brown, 2013). The list of contaminants generally includes particulate matter, condensable hydrocarbons (i.e. tars), sulfur compounds, nitrogen compounds, alkali metals (primarily potassium and sodium) and hydrogen chloride (Koido and Iwasaki, 2018). Cleaning requirements depend on the end use of the gas produced and/or emission standards: although ICEs are considered more tolerant to contaminants than gas turbines, a multi-step process is mandatory to tailor the quality of the raw syngas to the specifications of any power generator (Le Coq and Ashenafi, 2012).

### 1.4. Power generation from syngas

The prime movers for accomplishing the above mentioned "secondary conversion" have been analyzed extensively but separately in the published literature, either through simulation models, experimental work or a combination of both. From a theoretical point of view, Indrawan et al. (2020) provided a broad overview of power generation technologies suitable for using syngas derived from biomass gasification. They concluded that natural gas ICE is the most preferred for syngas applications, followed by gasoline and diesel engines; mGT was defined as an evolving technology that can achieve robust performance with syngas fuels with minimal modifications. Both ICEs and mGTs have been identified as the most suitable solutions to support distributed generation: they can provide fast start up, excellent load-following characteristics and low control complexity. However, power derating occurs when converting low-LHV syngas to electricity, as documented in the subsections below.

#### 1.4.1. Internal combustion engine

Bates and Dölle (2017) made clear that ICEs are derated by about 15%–40% when operated on syngas rather than petroleum fuels. In particular, power derating is less significant in gasoline or natural gas engines, with respect to homogeneous charge spark-ignition engines (Fiore et al., 2020). However, these require very little modification to run on syngas, such as advancing ignition timing because of low flame speed of syngas as compared to gasoline. On the other hand, compression ignition engine would operate more efficiently but a means is needed to initiate combustion because the temperature at the end of the compression stroke is lower than the self-ignition temperature of syngas (Pradhan et al., 2015). That is why a dual-fuel mode is adopted: diesel fuel is used as the pilot fuel, and syngas is introduced through the engine intake air and provides most of the fuel charge, up to 70–90% (Uma et al., 2004). When it comes to retrofitting an existing gasoline or natural gas engine to run on 100% syngas, Raman and Ram (2013) concluded that the latter involves minimal modification because it has an adequate compression ratio and is already equipped with a spark ignition system and a governor mechanism to control the throttle valve. Nevertheless, a tailor-made intake manifold is needed for air and syngas supply in the appropriate ratio, as the gas-to-air ratio of syngas (1:1.2) is very different from that of NG (1:13.5). In addition, the inlet pressure in natural gas engines is positive, whereas the syngas pressure at the engine intake is generally below the atmospheric level (Caligiuri et al., 2021).

As far as the environmental impact is concerned, Fiore et al. (2020) took stock of engine emissions when fossil fuels are replaced by syngas. The latter always leads to larger $CO_2$ content in the exhaust gas whereas the level of hydrocarbon is negligible. However, the benefits of syngas in terms of reducing CO and $NO_x$ emissions compared to NG (see, for example Gobbato et al. (2015)) are not always guaranteed, as shown by the results obtained by Mustafi et al. (2006). Trends found for these emissions are difficult to generalize, as they are influenced by operating parameters such as compression ratio, ignition timing and cylinder temperature (Hagos et al., 2014).

#### 1.4.2. Micro gas turbine

Syngas, composed of hydrogen and carbon monoxide, can provide stable operation when fed to a mGT in partial or full replacement for NG, according to experimental combustion testing (Lee et al., 2010; Corrêa et al., 2019). However, the LHV of syngas may result in adjusting the operating parameters in NG-designed mGTs to ensure turbine-compressor matching, while reducing the performance penalty: since an increase in compressor pressure ratio ($\beta_C$) combined with a reduction in turbine inlet temperature (TIT) is not rewarding, it is recommended to reduce the rotational speed (Liu and Weng, 2009). Mărculescu et al. (2016) thoroughly investigated the thermodynamic aspects of mGT adaptation to syngas use. At constant heat input in the combustion chamber, the lower the LHV of the syngas, the larger the flue gas flow rate. This is advantageous in terms of higher effectiveness of the recuperator (ε), when its exergetic efficiency is assumed to be a constant value of 0.9. However, the energy consumption of the fuel compressor (FC) increases with the flow rate of syngas fed to the burner, up to about 30% of the gross power in the case of syngas with a LHV of 4.3 MJ/Nm$^3$. As a result, net electrical output and efficiency decrease compared with the use of NG. A loss in mGT $\eta_{el,n}$ is confirmed by Corrêa et al. (2019) and Renzi et al. (2017), when syngas replaces 50% or 100% of NG destined for the combustor, respectively. Regarding the recuperator, ε is enhanced and the heat exchanged is reduced when syngas is used (Nicolosi and Renzi, 2018). But this is not a general conclusion since ε is affected by case-specific variation of air and exhaust flow rate, as well as exhaust temperature and composition.

Exhaust emissions are closely related to syngas composition: the larger the hydrogen content, the higher the $NO_x$ production (Othman and Boosroh, 2016). When dealing with CO, part load or idle mode operation may cause higher emission due to low combustion efficiency (Lee et al., 2010). Nevertheless, above 70% load, emissions of CO, NO and unburned hydrocarbons are very low for any mixture of NG and syngas. When compared to a gas engine of similar size, the mGT produces over 200 times less CO, 15 times less unburned hydrocarbons, and 3 times less NO per volume of the dry exhaust gas at the same $O_2$ content (Rabou et al., 2008).

### 1.5. Original contribution

The novelty of the paper arises from modeling a dual BtE chain in which syngas produced in a downdraft gasifier, after cleaning, is sent either to an ICE or to a mGT, having the same size when NG-fired (Fig. 1). This allowed a fair comparison of CHP performance, with a focus on the overall pathway from biomass to electricity and heat. It is evident from the literature review on biomass gasification over the past 20 years that ICE prevails over the mGT alternative in experimental installations as well as in theoretical studies (see Table 1). However, to the authors' knowledge, a direct and comprehensive comparison between the two prime movers, all boundary conditions being equal, has rarely been addressed. And this is even more true when part load conditions are dealt with, in a load-following operating mode. Indeed, Hadi Jafari and Kowsary (2014) compared ICE with mGT fueled by woody biomass syngas, with the aim of highlighting the most promising solution from both thermodynamic and economic point of view. They found

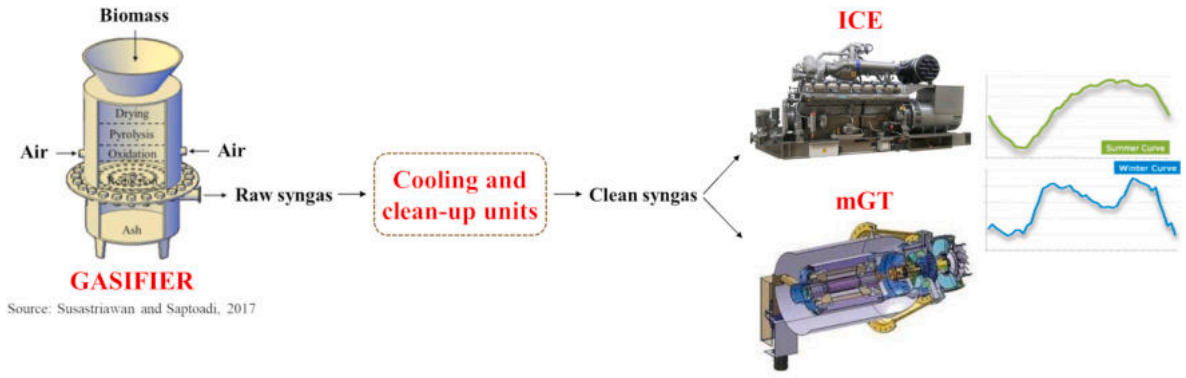


**Fig. 1.** Simplified representation of the proposed BtE chain.

**Table 1**
Literature review on ICEs and mGTs fueled by biomass syngas.

| | ICE | mGT |
|---|---|---|
| Experimental investigation | Sridhar et al. (2005)<br>Dasappa et al. (2011)<br>Lee et al. (2013)<br>Raman and Ram (2013)<br>Gabbrielli et al. (2016)<br>Elsner et al. (2017)<br>Vargas-Salgado et al. (2022) | Rabou et al. (2008)<br>Corrêa et al. (2019) |
| Theoretical modeling | Boloy et al. (2011)<br>Chang et al. (2019)<br>Copa et al. (2020)<br>Quintero et al. (2021) | Renzi et al. (2017)<br>Mărculescu et al. (2016) |

that an ICE integrated with an ambient pressure gasifier is the best option, whatever the size. In fact, three sizes of 100 $kW_{el}$, 1 $MW_{el}$ and 5 $MW_{el}$ were considered, albeit under full-load conditions. Therefore, the combined impact of fuel and load flexibility on each generator is the strength of this modeling study.

## 2. Modeling and validation of power plant sections

The power plant, based on biomass gasification and small-scale generation by either ICE or mGT, was modelled by means of Thermoflex® commercial code (version 30), under steady state conditions. The complete layout at nominal conditions is depicted in Figs. 2 and 3, respectively. Enthalpy, temperature, pressure and mass flow rate were

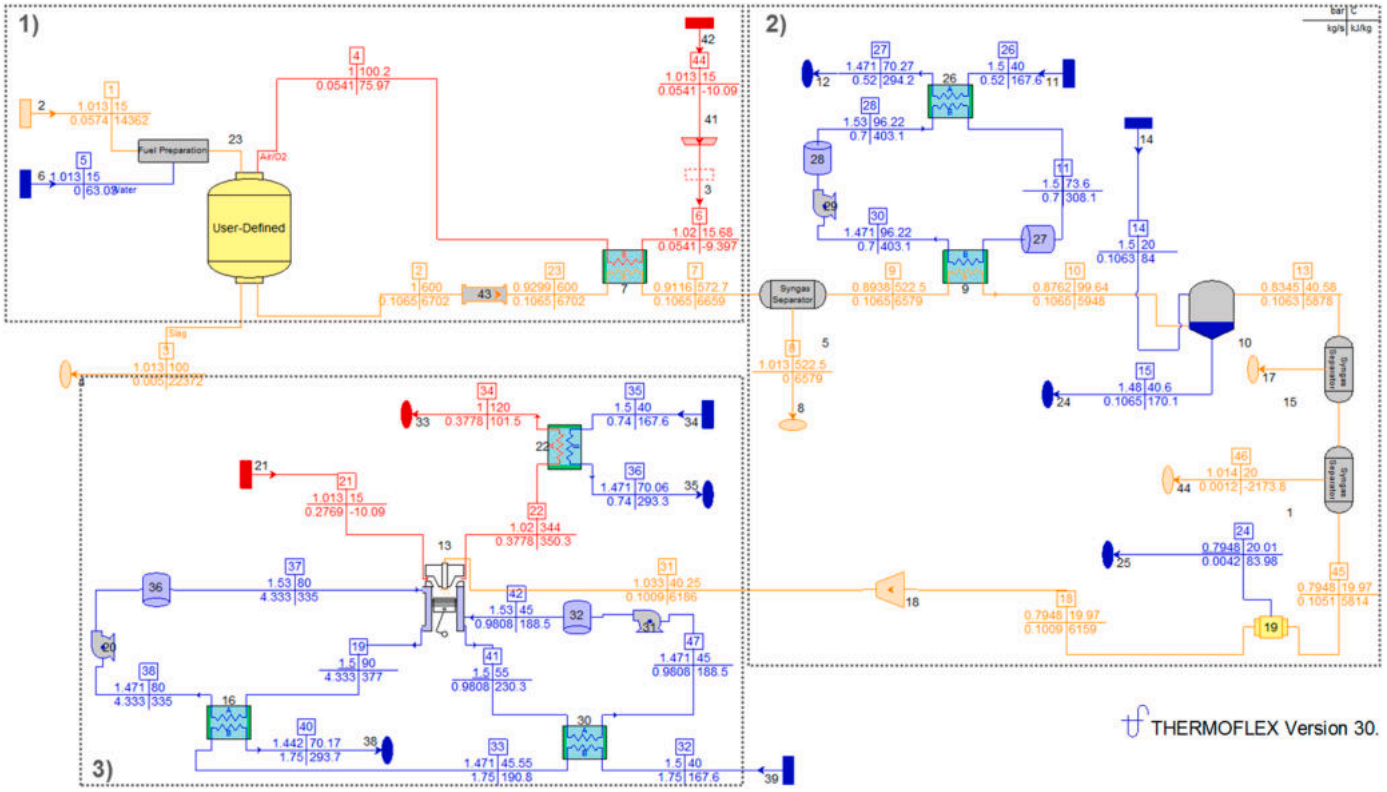


**Fig. 2.** Process flow diagram of the biomass power plant with ICE: 1) gasification, 2) syngas cleanup and 3) CHP generation (component numbers are written in black; stream numbers are shown in the boxes and also listed in Table B1.).

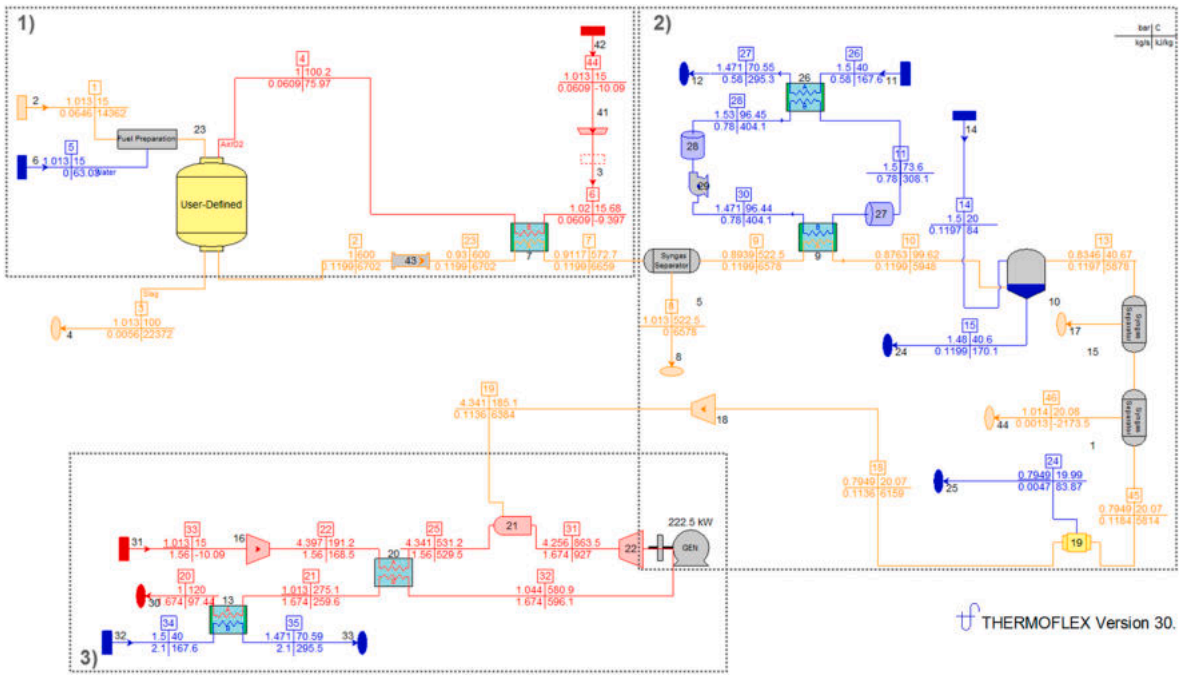


**Fig. 3.** Process flow diagram of the biomass power plant with mGT: 1) gasification, 2) syngas cleanup and 3) CHP generation (component numbers are written in black; stream numbers are shown in the boxes and also listed in Table B2.).

calculated upstream and downstream of each component, with a convergence tolerance within $10^{-4}$, for four consecutive loops. For the sake of clarity, the plant has been divided into three main sections: 1) gasification, 2) syngas cleanup and 3) CHP generation (ICE/mGT). For each section, modeling assumptions, design process and practices for validation and verification of simulation results were explained. It is important to mention that Sections 1 and 2 were conceived drawing inspiration from Elsner et al. (2017) because of the completeness of the information provided in terms of process flow diagram (Fig. A1) and related operational parameters (Fig. A2). These, being the result of both experimental and numerical analyses, were taken as the reference for validation. As regards the prime mover, manufacturer's specifications were the most significant source of data for evaluating the accuracy of predictions.

### 2.1. Gasification

Starting from Section 1, the user-defined component (23) was chosen to facilitate modeling of an ambient pressure, downdraft (fixed-bed) gasifier where the gasifying agent is preheated air with product gas sensible heat. Syngas outlet temperature, set at 600 °C, is reduced to about 570 °C by passing through the heat exchanger (7) where ambient air is heated to nearly 100 °C. Main input parameters included the following: CCE of 85% in line with Thomson et al. (2020); equivalence ratio of 0.25; air-fuel ratio (A/F) of 1.27. The equilibrium mode, based on a predefined set of equilibrium reactions, was used to predict the syngas composition, similarly to previous studies on large-scale gasifiers (Olivieri and Ravelli, 2020; Ravelli, 2021). *Bambusa oldhamii Munro*, which is a woody bamboo species, was chosen among high volatile content fuels. In general, bamboo has become a feedstock of potential interest for future energy production due to its high productivity and short rotation time (Wi et al., 2017). In particular, the species selected in this work seems to have the best qualities to feed a downdraft gasifier, according to Salovaara et al. (2015). They provided the ultimate and proximate analysis, collected in Table 2, by experimental testing. In detail, ash content, volatile matter and fixed carbon were determined through D3174, D3175 and D3172 ASTM standard methods, respectively. D5373 was applied to quantify carbon, hydrogen and nitrogen content whereas the method D4239 was used for sulfur. The amount of oxygen was obtained by balance calculations.

**Table 2**
Ultimate and proximate analysis of biomass fuel (Salovaara et al., 2015).

| Bambusa oldhamii Munro (bamboo species) | Wet (%wt.) | Dry (%wt.) |
|---|---|---|
| C | 39.70 | 46.70 |
| H | 5.18 | 6.09 |
| N | 0.07 | 0.08 |
| S | 0.04 | 0.05 |
| O | 37.23 | 43.80 |
| Moisture | 15% | – |
| Volatile | 66.98 | 78.80 |
| Ash | 2.79 | 3.28 |
| Char | 15.23 | 17.9 |
| LHV (kJ/kg) | 14,381 | |
| HHV (kJ/kg) | 15,878 | |

Slagging and acid gas production should not be a major problem due to the low content of ash and sulfur. The moisture content of 15% is within the upper limit for a downdraft gasifier. The LHV of 14,381 kJ/kg was calculated by the following correlation, which estimates the higher heating value (HHV):

$$HHV\ (kJ/kg) = 2.326\ [146.58\ C + 568.78\ H + 29.45\ S - 6.58\ A – 51.53\ (O + N)] \quad (1)$$

**Table 3**
Validation of raw syngas properties at the gasifier outlet.

| Parameter | Simulation | Salovaara et al. (2015) | Δ% |
|---|---|---|---|
| CO (% vol) | 14.86 | 14.99 | −0.9 |
| $CO_2$ (% vol) | 15.76 | 15.91 | −0.9 |
| $H_2$ (% vol) | 24.56 | 22.63 | 8.5 |
| $H_2O$ (% vol) | 9.33 | 8.74 | 6.8 |
| $CH_4$ (% vol) | 4.01 | 3.65 | 10.0 |
| $N_2$ (% vol) | 31.01 | 34.08 | −9.0 |
| Others (% vol) | 0.47 | – | – |

where C, H, S, A, O, and N are weight percentages, on a wet basis, of carbon, hydrogen, sulfur, ash, oxygen, and nitrogen, respectively. It deserves to be mentioned that Salovaara et al. (2015). experimentally investigated the HHV according to the D5865 standard, to validate Eq. (1).

Composition and LHV of the raw syngas at the gasifier outlet were verified against those reported in Salovaara et al. (2015), since their approach is similar to that used in this study (Table 3). The simulation delivered satisfactory results despite a slight overprediction of $H_2$ and $H_2O$ content. The major error concerns $CH_4$ concentration, which, however, is marginal, on the order of 4%. The equilibrium gasification model can be the reason behind the overestimation of $CH_4$ molar fraction, at low ER (Moretti et al., 2021). The same applies to the overestimation of $H_2$ content, regardless of the operating conditions of the gasification process. The raw syngas LHV is 5845 kJ/kg at the reference temperature of 25 °C, resulting in a reasonable CGE of 75.4%.

### 2.2. Syngas cleanup

The cleanup section was simulated by prioritizing changes in pressure, temperature, flow rate and syngas composition, across each component. Chemical/physical processes that may be required to achieve the removal of contaminants were not modelled, only their net effect on thermodynamic parameters. The first component is a syngas separator (5) that functions like a cyclone to trap fine ash impurities while lowering pressure and temperature of the syngas stream. Pressure drop amounts to dp/p = 2%, according to the following:

$$\frac{dp}{p} = \frac{p_{in}}{p_{out}} - 1 \tag{2}$$

$p_{in}$ and $p_{out}$ are the pressure values before and after the loss, respectively. With a heat rejection of 80 kJ/kg, syngas temperature drops by 50 °C. The syngas is subsequently cooled to about 100 °C (see component 9): the discharged heat is recovered through an intermediate circuit where hot water transfers thermal energy to the end-user, by means of component 26. Values of supply and return water temperature were set at 70 °C and 40 °C, respectively. Both heat exchangers (9 and 26) have a pressure drop of dp/p = 2% on each side and a normalized heat loss of 1%. Syngas is furtherly cooled to about 40 °C in a wet scrubber (icon 10) where solid particles and chlorine are removed simultaneously. Relative humidity of syngas leaving the scrubber was assumed to be 100%; syngas pressure drop is dp/p = 5%. Please note that the oil scrubber proposed by Elsner et al. (2017) in Fig. A1 was not included in the model. Subsequently, the syngas enters a pair of syngas separators (15, 1) whose removal efficiency is 80% and 95% for $H_2S$ and $NH_3$, respectively. Moreover, the water vapor extraction rate was set at 15%, with the purpose of mimicking the operation of a sand bed filter. This can ensure removal efficiency of tar and particulate in the range of 83–97%, despite causing slight wetting of the sand bed: the consequent percentage reduction of syngas moisture content by the filter was found between 10% and 18%, according to the experimental study by Pathak et al. (2007).

Le Coq and Ashenafi (2012) stated that bed filter units, combined with water quenching, can meet the syngas quality requirements for use in power generators, where the acceptable tar content must be lower than 100 mg/Nm$^3$.

With a heat rejection of 151.5 kJ/kg, the syngas temperature is reduced to 20 °C, with a total pressure drop of dp/p = 5%. Finally, a moisture separator (19) removes liquid water from the gas stream: as a result, the moisture fraction in the syngas decreases by about 4 percentage points (pp), from 6.2% to 2.3%. At that point, the syngas is composed of CO = 15.8%, $CO_2$ = 16.9%, $CH_4$ = 4.3%, $H_2$ = 26.2%, $H_2O$ = 3.0% and $N_2$ = 33.5 thus leading to a LHV of 6165 kJ/kg. After being cooled to near room temperature and purified, the syngas is sent to the FC (18), whose design pressure ratio ($\beta_{FC}$) depends on the downstream power system. In the case of ICE, $\beta_{FC}$ of 1.3 is sufficient to compensate for pressure losses along the cleanup section by returning the syngas pressure to about ambient level. In the case of mGT, a nominal $\beta_{FC}$ of 5.5 is required to feed the combustor at full load. In both cases, FC design polytropic efficiency was set at 75%, consistently with Hadi Jafari and Kowsary (2014), whereas mechanical efficiency is equal to 95%.

### 2.3. CHP generation

Each power system was selected to meet the desired capacity, i.e. 200 $kW_{el,n}$, and modelled in stand-alone configuration, corresponding to Section 3 of Figs. 2 and 3, before being included in the flow diagram of the overall plant in off-design mode. Part load performance was evaluated with both NG and syngas to assess possible reductions in power and efficiency due to fuel switching.

#### 2.3.1. ICE

A Siemens gas engine (SGE) was chosen as a flexible generator, in terms of fuel and load acceptance. In particular, the model SGE-18SL, with a speed of 1200 rpm, fits the purpose of this study: its main characteristics, collected in Table 4, were taken from Siemens Energy (2017a). Fig. 4 shows an enlarged view of the engine model, with all the components needed to simulate the heat recovery from exhaust gas (cooled to 120 °C), jacket water combined with oil cooler and intercooler water. The definition of the engine operating parameters at full load, with NG as fuel, was carried out by implementing the customized inputs of Table 4 through a user-defined configuration, as recommended by Chang et al. (2019). However, the pre-built engine model available in Thermoflex®, which is the SGE-18SL with a speed of 1500 rpm and electrical power ($P_{el}$) of 304 $kW_{el}$, was useful to deduce the part load behavior, assuming that the exhaust temperature remains constant at the design value (344 °C).

Replacing NG with syngas, for the same fuel energy input, implied a reduction in power rating from 241 to 199 $kW_{el}$, as stated by the manufacturer (Siemens Energy Inc., 2017b). It was assumed that the electrical efficiency ($\eta_{el}$) decreases constantly, by about 18%, when the load drops from 100% to the minimum value of 40%. This approach provided realistic performance for the selected engine when compared with the manufacturer's stated operating conditions, regardless of fuel

**Table 4**
Engine specifications with NG as fuel (Siemens Energy Inc., 2017a).

| SGE-18SL (1200 rpm) turbocharged; single intercooler; aftercooled | | | |
|---|---|---|---|
| Electrical power ($kW_{el}$) | 241 | Jacket water & oil cooler heat ($kW_{th}$) | 182 |
| Cylinder arrangement | 6 L | Intercooler water heat ($kW_{th}$) | 41 |
| Mean effective pressure (bar) | 14 | Exhaust heat ($kW_{th}$) | 97 |
| Bore (mm) | 152 | Fuel input (kW) | 624 |
| Stroke (mm) | 165 | Mechanical efficiency (%) | 40.4 |
| Diaplacement (l) | 18 | Electrical efficiency (%) | 38.6 |
| Mean piston speed (m/s) | 6.6 | Thermal efficiency (%) | 51.3 |
| Compression ratio | 11.6:1 | Generator efficiency (%) | 95.5 |
| Jacket water temperature max (°C) | 90 | Intercooler coolant temperature max (°C) | 55 |
| Jacket water flow rate min/max ($m^3$/h) | 25/60 | Intercooler coolant flow rate min/max ($m^3$/h) | 15/30 |
| Exhaust temperature (°C) | 344 | Exhaust mass flow wet (kg/h) | 1360 |

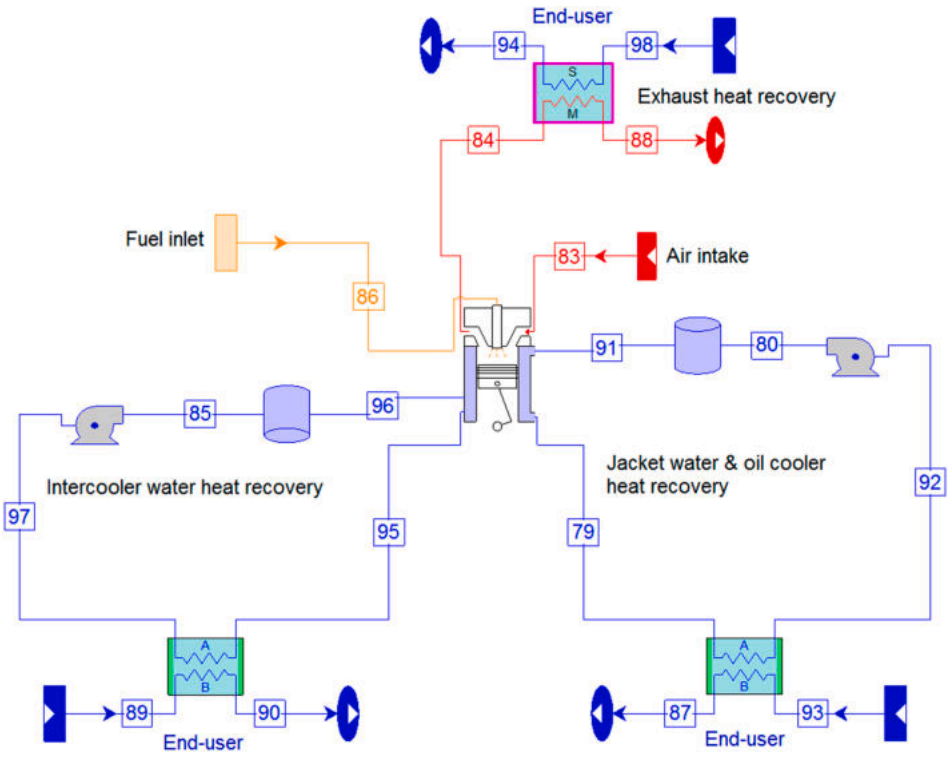


**Fig. 4.** CHP generation through ICE.

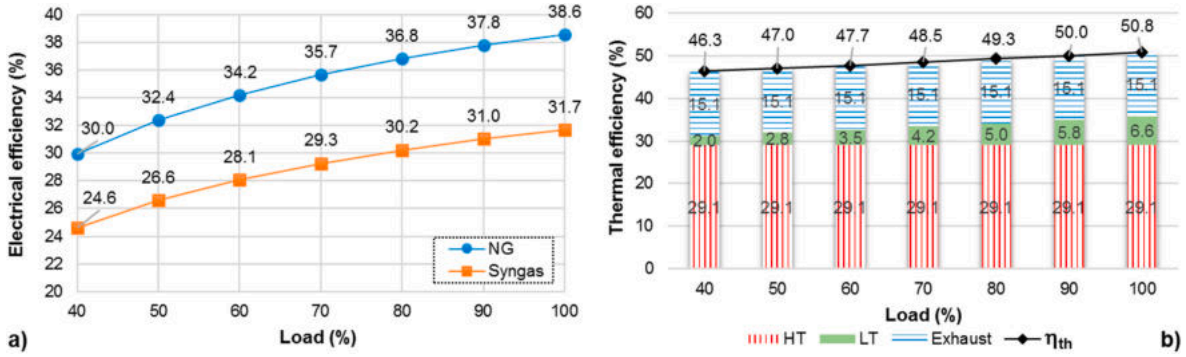


**Fig. 5.** ICE off-design performance at ISO conditions: (a) electrical efficiency; (b) thermal efficiency.

and load. Conversely, thermal efficiency ($\eta_{th}$), defined as the ratio of heat recovered to the chemical energy of the fuel, was not significantly affected by the fuel type: the penalty due to load reduction is within 4.5 pp regardless of fuel. Fig. 5 summarizes the off-design performance of the ICE, under varying load and fuel, in terms of $\eta_{el}$ (Fig. 5a) and $\eta_{th}$ (Fig. 5b). It is clear that NG achieves $\eta_{el}$ in the 30–39% range whereas levels of $\eta_{el}$ are lowered to 25–32% when syngas is used. Values of $\eta_{th}$ vary from 46% to 51%: its degradation at part load is mainly due to less effective heat recovery from the intercooler water heat, in the so-called low temperature (LT) circuit. On the opposite, heat recovery from high temperature (HT) jacket water and exhaust gas ensures a stable contribution of 29% and 15%, respectively, to $\eta_{th}$, whatever the load. As to the latter point, it should be noted that the exhaust flow rate decreases with load (from 0.378 at 100% load to 0.195 kg/s at 40% load) but does not vary with fuel. Therefore, A/F is about 27 for air-NG mixture vs. 2.7 for air-syngas mixture, at any load.

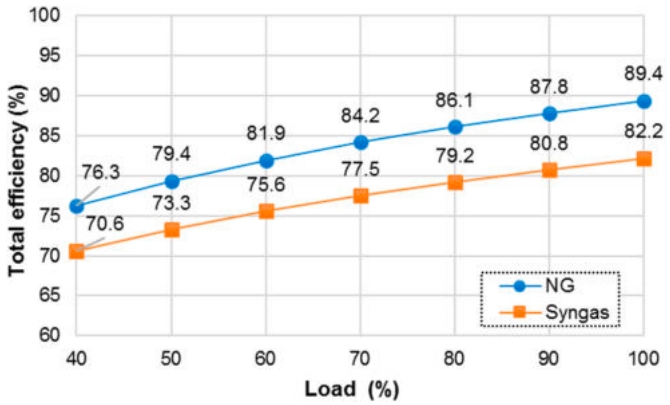


**Fig. 6.** ICE off-design performance at ISO conditions: total efficiency.

The total efficiency ($\eta_{tot}$), commonly defined as the sum of electrical and thermal output divided by the fuel energy input, is represented in Fig. 6. Although syngas is detrimental to $\eta_{tot}$, the calculated range from 71% to 82% is still remarkable.

### 2.3.2. mGT

Features of the Capstone C200 (200 kW) mGT, chosen as a reference,

**Table 5**
mGT specifications with NG as fuel.

| Parameter | Simulation | Hampel and Braun (2022) | Δ% |
|---|---|---|---|
| Compressor isentropic efficiency ($\eta_{is,C}$ %) | 84.1 | | – |
| Preheated air temperature – $T_3$ (°C) | 580 | 578 | 0.3 |
| Turbine inlet temperature (°C) | 954 | | – |
| Turbine isentropic efficiency ($\eta_{is,T}$) | 86.1 | | – |
| Turbine outlet temperature (°C) | 649 | 650 | −0.2 |
| Exhaust temperature – $T_6$ (°C) | 277 | 280 | −1.1 |
| Air flow rate (kg/s) | 1.590 | 1.287 | 23.5 |
| Fuel flow rate (kg/s) | 0.0159 | 0.0128 | 24.2 |

were modified to provide the same power output as the ICE: specifically, mass flow rate of air and NG was increased by about 24% to reach $P_{el}$ of 241 kW, while keeping the thermodynamic cycle unchanged. The choice of design parameters, listed in Table 5, was guided by the study of Hampel and Braun (2022). Fig. 7 helps to identify the main components of the regenerative mGT. In short, both compressor and turbine are single-stage, radial flow turbomachines with a nominal pressure ratio of $\beta_C = 4.3$ and $\beta_T = 4.04$, respectively. Given the isentropic efficiency ($\eta_{is}$) in Table 5, polytropic efficiency ($\eta_y$) was equal to $\eta_{y,C} = 86.8\%$ and $\eta_{y,T} = 83.8\%$. The recuperator effectiveness was set at $\varepsilon = 84.4\%$ so that compressed air is preheated to $T_3 = 580$ °C using heat from the turbine exhaust available at $T_5 = 650$ °C. Flue gas, which exits the recuperator at nearly 280 °C, is furtherly cooled to the final temperature of $T_7 = 120$ °C (as in the case of ICE) to enable hot water production. Pressure drops are contained in Table 6.

Mechanical efficiency of 99.25% was assumed for both compressor and turbine. With a rotation speed of 60,000 rpm, the single shaft power electronic interface (including high frequency generator, rectifier and inverter) was characterized by an overall efficiency of 83%, resulting from assigning 94% efficiency to each of three devices. Nominal performance of the NG fueled mGT is reported in Table 7: note that $\eta_{el}$ matches well with that stated in Capstone (2009), i.e. 33 (±2)%.

### 2.3.3. Part load strategy

Consistently with Hampel and Braun (2022), shaft speed was varied to meet the required load: as inlet air decreases, fuel flow is adjusted to keep the turbine outlet temperature (TOT) almost constant at the design value, given the limitations of the recuperator material (i.e. stainless steel). On the other hand, keeping the TIT at design value would have caused the TOT to exceed the upper limit as the load decreased. Other suggestions, from the same source, relate to off-design modeling of the recuperator and power electronics. In the former case, the overall heat transfer coefficient (U) and heat exchange area (A) are lumped as the conductance value (UA), to calculate the heat transfer rate as a function of the log-mean temperature difference between hot and cold fluids. Specifically, the program determines the off-design value of UA by applying the method of *multi-parameter thermal resistance scaling* (Thermoflex, 2023) to the design point UA using the off-design flow rates and fluid conditions such as temperature, pressure and molecular weight.

In the latter case, the following was applied to compute the efficiency of the power electronics ($\eta_{pe}$), starting from the design value of $\eta_{pe,D} = 83\%$.

$$\eta_{pe} = \eta_{pe,D}\left[2.1186\left(\frac{P_{el}}{P_{el,D}}\right)^5 - 9.1014\left(\frac{P_{el}}{P_{el,D}}\right)^4 + 15.017\left(\frac{P_{el}}{P_{el,D}}\right)^3 - 11.972\left(\frac{P_{el}}{P_{el,D}}\right)^2 + 4.6771\left(\frac{P_{el}}{P_{el,D}}\right) + 0.2601\right] \quad (3)$$

For the compressor and turbine, the relationship between pressure ratio ($\beta_C$, $\beta_T$) and the corrected flow, with lines for each value of corrected speed, was implemented through performance maps, according to a method used successfully in a previous study (Bonasio and Ravelli, 2022). The reader is referred to that article for a detailed explanation of the parameters involved and the procedure adopted, which are valid for any mGT model. The main outcome is the mGT equilibrium-running line, in which compressor-turbine matching is guaranteed under any

**Table 6**
mGT normalized pressure loss at design point.

| Component | Δp/p (%) |
|---|---|
| Combustor | 2 |
| Recuperator – air side | 1.4 |
| Recuperator – exhaust side | 3.0 |
| Recovery heat exchanger – exhaust side | 1.3 |
| Recovery heat exchanger – water side | 2 |

**Table 7**
mGT nominal performance with NG as fuel.

| Parameter | Simulation |
|---|---|
| Electrical power ($kW_{el}$) | 241 |
| Fuel input (kW) | 735 |
| Exhaust heat ($kW_{th}$) | 262 |
| Electrical efficiency % | 32.9 |
| Thermal efficiency % | 35.5 |

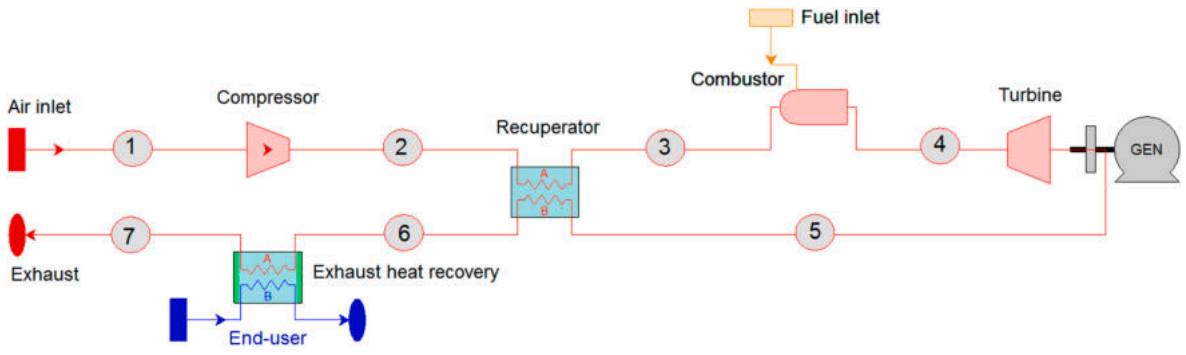


**Fig. 7.** CHP generation through mGT.

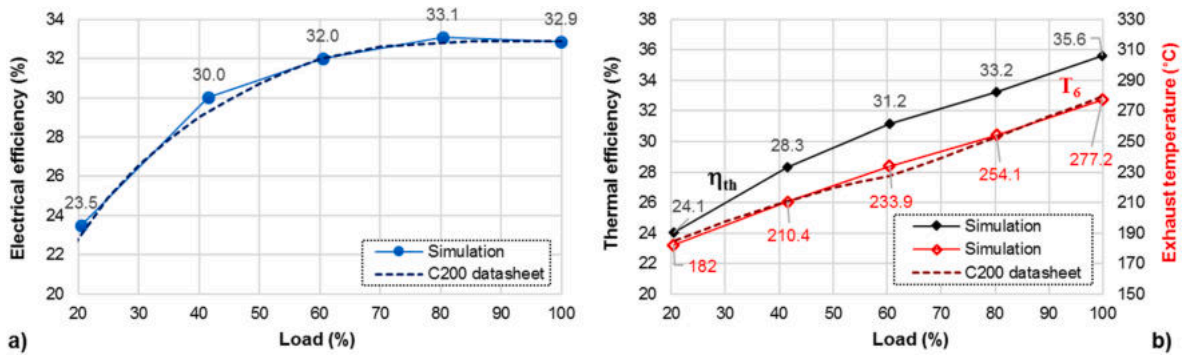


**Fig. 8.** mGT off-design performance at ISO conditions, with NG as fuel: (a) electrical efficiency; (b) thermal efficiency.

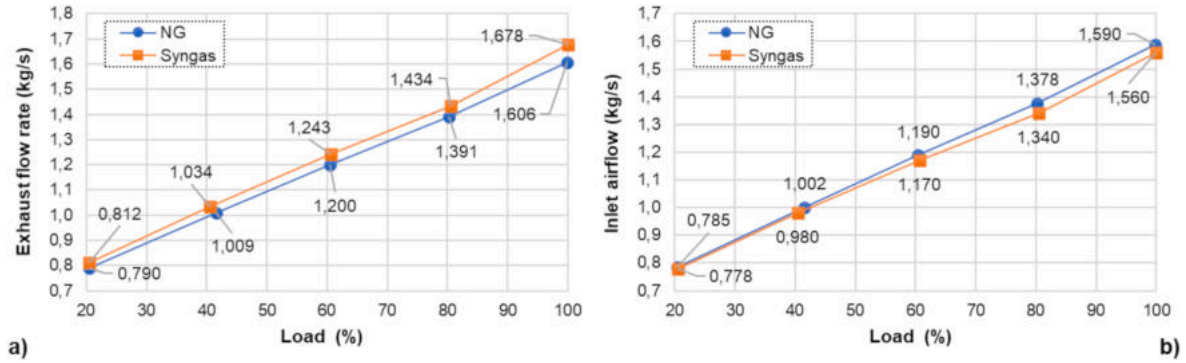


**Fig. 9.** Impact of fuel type at different load levels, from 20% to 100%, on mGT: (a) exhaust flow rate; (b) inlet airflow.

off-design condition. It is fair to point out that the performance maps applied here were adapted from those of Turbec T100 (see Caresana et al., 2014), due to the lack of specific data for Capstone C200. For an explanation of the applied procedure, the reader is referred to Appendix C. However, this did not affect the accuracy of the results, as shown in Fig. 8a: predicted values of $\eta_{el}$, with NG as fuel, differ by no more than 4% from those stated by the manufacturer, for the load range of 20–100%. The degradation in $\eta_{el}$, within 9.4 pp, is accompanied by a worsening of $\eta_{th}$, due to a reduced exhaust flow entering the recovery heat exchanger at decreasing temperature (Fig. 8b). Indeed, the declining trend in $T_6$ is in excellent agreement with the manufacturer's data.

The five operating points shown in Fig. 8, at 20% load step, were recalculated by replacing NG with syngas, with the same fuel energy input to the combustor. Therefore, a larger amount of syngas must be burnt, compared to NG, to compensate for the difference in LHV: the increase in the exhaust flow rate ranges from 2.8 pp at 20% load to 4.5 pp at full load (Fig. 9a). Hence, greater exhaust flow enters the turbine at reduced TIT thus resulting in higher $\beta_T$. The compressor adapts to provide higher $\beta_C$ by lowering its corrected flow, hence inlet airflow. This is reduced within a maximum of 3%, compared with the case with NG (Fig. 9b).

These changes affected the mGT running line as evident from Fig. 10: fuel switching had a greater impact on compressor than on turbine in terms of corrected flow, as expected. Nevertheless, small variations in $\eta_y$ were found whatever the turbomachinery.

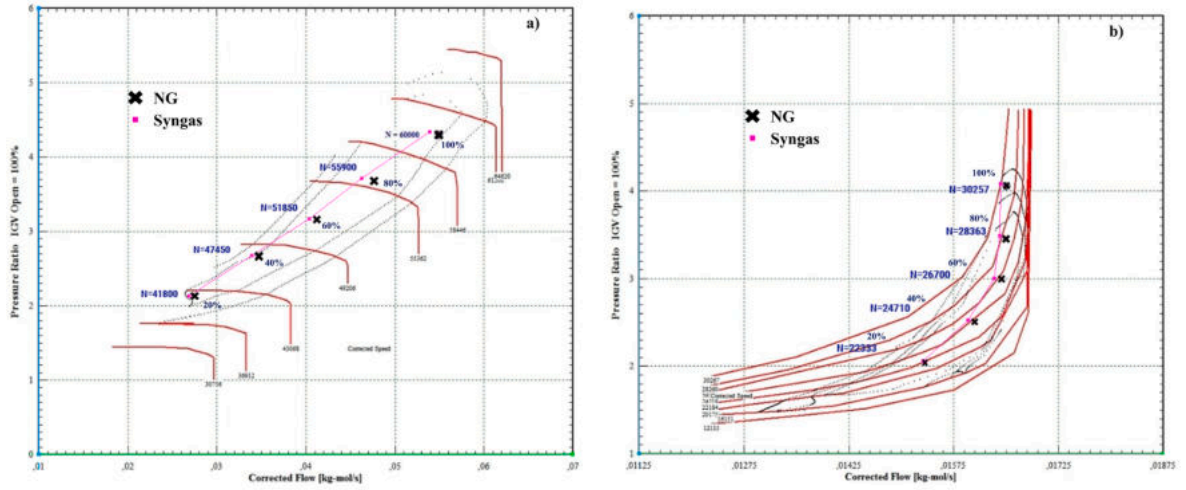


**Fig. 10.** Impact of fuel type at different load levels, from 20% to 100%, on performance maps of: (a) compressor; (b) turbine. N refers to corrected speed.

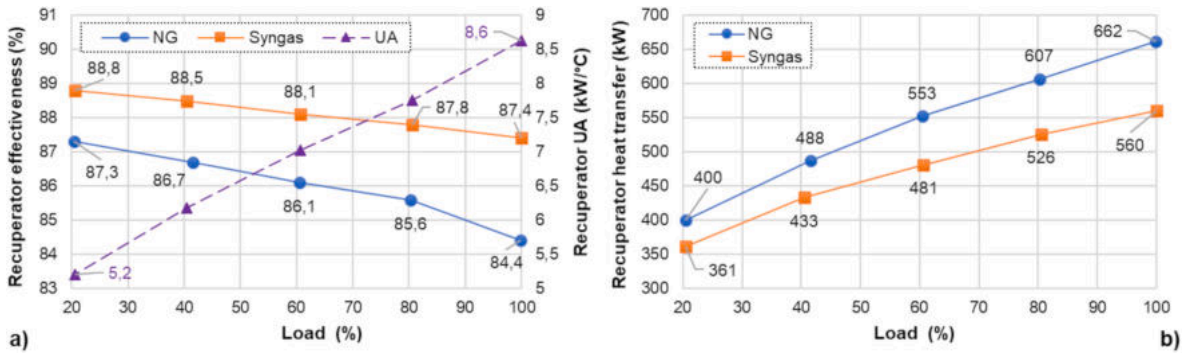


**Fig. 11.** Impact of fuel type at different load levels, from 20% to 100%, on recuperator performance in terms of: (a) effectiveness and UA; (b) heat transfer.

**Table 8**
mGT part load performance: NG vs. syngas.

| Shaft speed (rpm) | | NG | Syngas | NG | Syngas | NG | Syngas | NG | Syngas |
|---|---|---|---|---|---|---|---|---|---|
| | Load (%) | $P_{el}$ (kW) | $P_{el}$ (kW) | $\eta_{el}$ (%) | $\eta_{el}$ (%) | $\eta_{th}$ (%) | $\eta_{th}$ (%) | $\eta_{tot}$ (%) | $\eta_{tot}$ (%) |
| 60,000 | 100 | 241 | 223 | 32.9 | 30.3 | 35.6 | 37.1 | 68.5 | 67.4 |
| 55,900 | 80 | 193 | 179 | 33.1 | 30.6 | 33.2 | 34.6 | 66.3 | 65.2 |
| 51,850 | 60 | 146 | 135 | 32.0 | 29.6 | 31.2 | 32.2 | 63.2 | 61.8 |
| 47,450 | 40 | 100 | 90 | 30.0 | 27.0 | 28.3 | 30.1 | 58.4 | 57.1 |
| 41,800 | 20 | 49 | 46 | 23.5 | 21.8 | 24.1 | 24.6 | 47.6 | 46.4 |

As for the recuperator, higher exhaust flow on the hot side combined with lower air flow on the cold side resulted in improved performance (Fig. 11a): ε increases by 1.5–3 pp, with the benefit becoming more substantial as load increases, in full agreement with Mărculescu et al. (2016).

Fig. 11a also shows the linear decrease in conductance with load: UA reaches the highest value of 8.6 kW/°C, at the design point; at the lowest load, it drops to 5.2 kW/°C. These values refer approximately to both fuel cases (that is why a single UA curve has been reported). With the support of Fig. 11b, the following can be deduced: heat transfer through the recuperator is higher with NG but ε is lower. In other words, the use of syngas reduces the heat transfer but ε is enhanced. These trends are consistent with Nicolosi and Renzi (2018), whatever the load. They argued that reducing the cold medium flow (air) can facilitate the heat transfer process because the recuperator is "oversized", but the total amount of exchanged heat is lowered.

Table 8 focused on the impact of fuel type on mGT performance at discrete load levels. Focusing on electrical output, power derating on the order of 7% was confirmed at any load when using syngas instead of NG. Accordingly, the reduction in $\eta_{el}$ was estimated to be between 1.7 and 3 pp. This is the best that can be achieved in view of the fact that the higher exhaust flow rate, due to syngas feeding, is available at lower temperatures at the turbine inlet, as dictated by the combustor heat balance (Fig. 12): the difference between the reported TIT profiles is more pronounced the higher the load value.

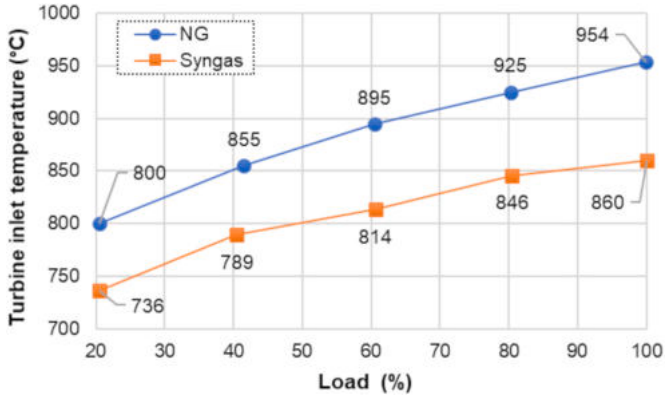


**Fig. 12.** Impact of fuel type at different load levels, from 20% to 100%, on turbine inlet temperature.

On the opposite, syngas has improved $\eta_{th}$ (within 2 pp) thanks to the increased exhaust flow, at almost unchanged $T_6$. However, this is not sufficient to compensate for the decrease in $\eta_{el}$ therefore $\eta_{tot}$ is lower than that with conventional fuel, albeit slightly.

## 3. Modeling and simulation of the whole BtE chain

The plant sections described above, after being properly validated, were combined into the layout of Figs. 2 and 3 in order to assess the overall system performance. It should be clarified that gross electrical power ($P_{el,g}$) is the electrical output of the generator (ICE/mGT) whereas net electrical power ($P_{el,n}$) is equal to:

$$P_{el,n} = P_{el,g} - P_{el,aux} \tag{4}$$

where $P_{el,aux}$ accounts for the consumption of auxiliary services. The overall net electrical efficiency was computed from the biomass energy input ($P_{fuel}^{(b)}$) according to:

$$\eta_{el,n}{}^{(b)} = \frac{P_{el,n}}{P_{fuel}^{(b)}} \tag{5}$$

Conversely, the following:

$$\eta_{el,g}{}^{(s)} = \frac{P_{el,g}}{P_{fuel}^{(s)}} \tag{6}$$

where $P_{el,g}$ is divided by the energy input from syngas, labeled as $P_{fuel}^{(s)}$, quantifies the performance of the generator within the BtE process, for comparison with the results in stand-alone configuration of Sections 2.3.1 and 2.3.2. Alternatively, the FC can be considered as an auxiliary system integrated into the prime mover, according to:

$$\eta_{el,n}{}^{(s)} = \frac{P_{el,g} - P_{FC}}{P_{fuel}^{(s)}} \tag{7}$$

Thermal and total efficiency were defined as follows:

**Table 9**
BtE chain performance at full capacity (ISO conditions): ICE vs. mGT.

| Parameter | BtE chain – ICE | BtE chain – mGT |
|---|---|---|
| Biomass flow rate (kg/s) | 0.057 | 0.065 |
| Biomass fuel input ($P^{(b)}_{fuel}$) (kW) | 825 | 929 |
| Clean syngas flow rate (kg/s) | 0.101 | 0.114 |
| Syngas fuel input ($P^{(s)}_{fuel}$) (kW) | 623 | 701 |
| Gross power ($P_{el,g}$) ($kW_{el}$) | 199 | 223 |
| Auxiliary power ($P_{el,aux}$) ($kW_{el}$) | 9.4 | 44.1 |
| • Fuel compressor | 4.8 | 38.9 |
| • Gasifier feed system | 4.5 | 5.1 |
| • Pumps and fans | 0.1 | 0.1 |
| Net power ($P_{el,n}$) ($kW_{el}$) | 190 | 179 |
| Thermal energy ($kW_{th}$) | 380 | 343 |
| • HT/LT circuit | 180/41 | – |
| • Exhaust | 93 | 269 |
| • Syngas cooling | 66 | 74 |
| Hot water recovery – flow rate (kg/s) | 3.01 | 2.7 |
| $\eta^{(s)}_{el,g}$ % | 32.0 | 31.8 |
| $\eta^{(s)}_{el,n}$ % | 31.2 | 26.3 |
| $\eta^{(b)}_{el,n}$ % | 23.0 | 19.2 |
| $\eta^{(b)}_{th}$ % | 46.0 | 36.9 |
| $\eta^{(b)}_{tot}$ % | 69.0 | 56.1 |

$$\eta_{th}^{(b)} = \frac{P_{th}}{P_{fuel}^{(b)}} \tag{8}$$

$$\eta_{tot}^{(b)} = \frac{P_{el,n} + P_{th}}{P_{fuel}^{(b)}} \tag{9}$$

Equation (9) provides the most comprehensive energy assessment of the proposed solutions, consistent with the so-called CHP approach.

The analysis was first carried out at ISO conditions, with ICE/mGT working at full and part load. The model was then exercised to predict the effects of load following: $P_{el,n}$ was adjusted as demand for electricity and ambient conditions fluctuate throughout the day, for two representative cases. Output variables were determined in hourly resolution.

### 3.1. Results at full load: ICE vs. mGT

Simulation outputs at full capacity were presented in Table 9 to allow consistent and immediate comparison between ICE and mGT, on the assumption of the same biomass fuel and clean syngas quality. The parameters that define the energy balance of the plant are given in the first section of the table, while the second one shows efficiency values. Difference in $P_{el,g}$ reflects the effect of derating, since both ICE and mGT were designed to deliver the same power output (241 $kW_{el}$) when fed by NG. Although $P_{el,g}$ is higher for mGT, ICE is better in terms of $P_{el,n}$ due to the much lower burden of auxiliaries. What makes the difference is undoubtedly the power absorbed by FC, which is one order of magnitude higher for mGT. This is due to higher $\beta_{FC}$ (5.5 vs. 1.3), as explained in Section 2.2, and slightly larger syngas flow rate at FC inlet. Consequently, more biomass is required in mGT case, which explains the slightly higher consumption of the gasifier feeding system, which includes conveyors elevators and loading hoppers. Water circulating pumps and gasifier air blower are responsible for a small amount of power absorbed in both cases, and their impact on auxiliary power consumption is negligible.

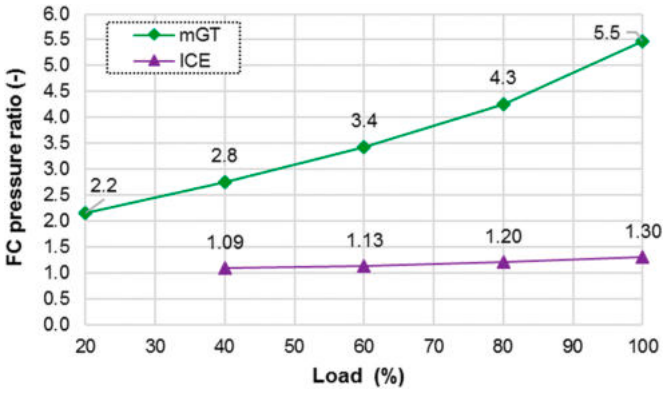


**Fig. 13.** FC pressure ratio ($\beta_{FC}$) at part load: ICE vs. mGT.

Moreover, ICE offers a greater amount of thermal energy, collected from four different sources (HT and LT circuit, exhaust and syngas cooling). In mGT case, heat is recovered only from exhaust and syngas cooling, albeit in larger quantities. This is especially true for the exhaust gas heat recovery, given the significantly higher exhaust flow rate (1.67 vs. 0.38 kg/s), although discharged at a lower temperature (275 vs. 344 °C).

Turning to efficiency, $\eta^{(s)}_{el,g}$ is a little higher than that reported in the previous sections for both ICE (32.0 vs 31.7%) and mGT (31.8 vs 30.3%): the reason may be found in the increased temperature of the inlet syngas fuel (40 °C for ICE; 185 °C for mGT), above the ISO standard reference of 15 °C, due to upstream compression in FC. That said, ICE has similar performance to mGT in terms of $\eta^{(s)}_{el,g}$. But when FC is taken into account, its power absorption severely penalizes the mGT causing about a 5-point drop in electrical efficiency, as demonstrated by $\eta^{(s)}_{el,n}$.

Overall, ICE was identified as the most appropriate solution in all respects when included in the BtE chain: the gain in $\eta^{(b)}_{tot}$, which is about 13 pp compared with mGT, can be roughly divided into 4 and 9 pp attributable to electrical and thermal performance, respectively. The validity of findings was further checked against the results by Hadi Jafari and Kowsary (2014): they stated that $\eta^{(b)}_{el,n}$ reaches almost 24% and

**Table 10**
BtE chain performance at part load (ISO conditions): ICE vs. mGT.

| Parameter | Load = 80% | | Load = 60% | | Load = 40% | |
|---|---|---|---|---|---|---|
| BtE chain parameter | ICE | mGT | ICE | mGT | ICE | mGT |
| Biomass flow rate (kg/s) | 0.048 | 0.052 | 0.039 | 0.041 | 0.030 | 0.030 |
| Biomass fuel input ($P^{(b)}_{fuel}$) (kW) | 693 | 745 | 559 | 583 | 426 | 428 |
| Clean syngas flow rate (kg/s) | 0.084 | 0.091 | 0.068 | 0.071 | 0.052 | 0.052 |
| Syngas fuel input ($P^{(s)}_{fuel}$) (kW) | 523 | 562 | 422 | 440 | 321 | 323 |
| Gross power ($P_{el,g}$) ($kW_{el}$) | 159 | 179 | 119 | 135 | 80 | 90 |
| Auxiliary power ($P_{el,aux}$) ($kW_{el}$) | 6.6 | 30.1 | 4.7 | 20.2 | 4.0 | 12.5 |
| • Fuel compressor | 2.8 | 26 | 1.6 | 17 | 1.6 | 10.1 |
| • Gasifier feed system | 3.8 | 4.1 | 3.1 | 3.2 | 2.4 | 2.4 |
| • Pumps and fans | <0.05 | <0.05 | <0.05 | <0.05 | <0.05 | <0.05 |
| Net power ($P_{el,n}$) ($kW_{el}$) | 153 | 149 | 115 | 115 | 76 | 78 |
| Thermal power ($kW_{th}$) | 313 | 270 | 250 | 212 | 188 | 156 |
| • HT/LT circuit | 151/26 | – | 122/15 | – | 93/7 | – |
| •Exhaust | 80 | 210 | 67 | 164 | 53 | 121 |
| • Syngas cooling | 56 | 60 | 46 | 48 | 35 | 35 |
| Hot water recovery – flow rate (kg/s) | 1.85 | 2.11 | 1.46 | 1.67 | 1.07 | 1.25 |

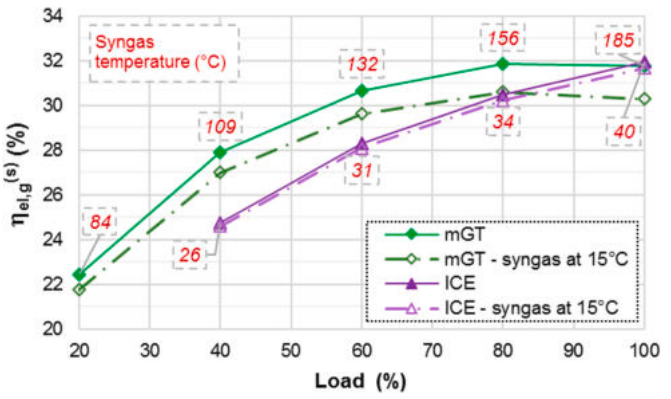


**Fig. 14.** Part load generator efficiency ($\eta_{el,g}^{(s)}$) as a function of syngas inlet temperature: ICE vs. mGT.

19% in the case of ICE and mGT, respectively, for a similar size of 100 $kW_{el}$.

### 3.2. Results at part load: ICE vs. mGT

The behavior of the power plant was then explored through multiple simulations reducing the load to the minimum allowed by each generator. Energy balance predictions were compiled in Table 10 at the load levels of 80–60–40%, for easy comparison. It should first be specified that gasification process was poorly affected by load change: the LHV of clean syngas may raise slightly, from 6165 kJ/kg at 100% load to 6225 kJ/kg at 40% load, but CGE remained within a few tenths of a percent, i.e. between 75.4 and 75.7%. A downward trend is observed in all reported parameters as the load is reduced, but with certain differences. In depth, the nearly linear decrease characterizing $P_{fuel}^{(b)}$, $P_{fuel}^{(s)}$ and $P_{el,g}$ is slightly steeper for the mGT cases, whose values exceed those of ICE at full load but fall to near engine performance at 40% load. Moreover, even though mGT is subject to larger auxiliary consumption than ICE over the entire load range, it benefited most from the reduction in the power absorbed by the FC, due to the favorable combined decrease in clean syngas flow rate and $\beta_{FC}$. This was plotted against load in Fig. 13. For mGT, $\beta_{FC}$ is roughly halved when load changes from 100% to 40%, so FC power requirement, computed as a percentage of $P_{el,g}$, falls from 17.5% to 11.2%, in line with Mărculescu et al. (2016). In ICE case, $\beta_{FC}$ declines gradually from 1.3 to 1.1 thus resulting in a minor impact of FC, less than 2.4%, compared to $P_{el,g}$. That is why mGT can provide comparable or even higher $P_{el,n}$ than ICE at load $\leq$60%. The role of FC is also fundamental in explaining the profiles of $\eta_{el,g}^{(s)}$ shown in Fig. 14: the higher the $\beta_{FC}$, the higher the temperature of the syngas entering the generator (see labels), which has a beneficial effect on its performance, compared with the results obtained at the reference temperature (15 °C). Hence, the gain in $\eta_{el,g}^{(s)}$ is negligible for ICE (within 0.3 pp) but noteworthy for mGT (between 0.7 and 1.5 pp). So, the latter outperforms the former when inserted into the BtE chain, except for the full load, and the gap grows as the load decreases. But the pattern is totally reversed when it comes to $\eta_{el,n}^{(s)}$, as shown in Fig. 15. The advantage in favor of using ICE, compared with the competitor, is maximum at full load and reduces to zero when the load is halved. This finds correspondence in the characterization of the entire BtE chain, when the focus shifts to $\eta_{el,n}^{(b)}$. FC makes the difference: it is necessary to lower the load below 50%, and with it $\beta_{FC}$, to see a slightly higher $\eta_{el,n}^{(b)}$ for mGT than for ICE (Fig. 16). In other words, the best-possible outcomes can be achieved by using ICE within half load, with $\eta_{el,n}^{(b)}$ ranging from 19% to 23%, and mGT at lower loads, with $\eta_{el,n}^{(b)}$ dropping from 19% to 13.5% at the minimum load of 20%. On the other hand, ICE emerged as a clear leader when dealing with thermal performance. It ensured not only the largest amount of total heat recoverable (see Table 10), primarily thanks to HT/LT circuit, but also the highest levels of $\eta_{th}^{(b)}$ across the whole load span (Fig. 16). Indeed, the range of 44.0–46.0% is much higher than that of mGT (35.4–36.9%). In both cases, curves of $\eta_{th}^{(b)}$ are relatively flat even though heat recovery is penalized by part load operation, in a linear manner. Values of $\eta_{el,n}^{(b)}$ and $\eta_{th}^{(b)}$ led to the definition of $\eta_{tot}^{(b)}$: it is between 61.7 and 69.0% for ICE whereas the range of 48.9–56.1% was computed for mGT, based on biomass energy input.

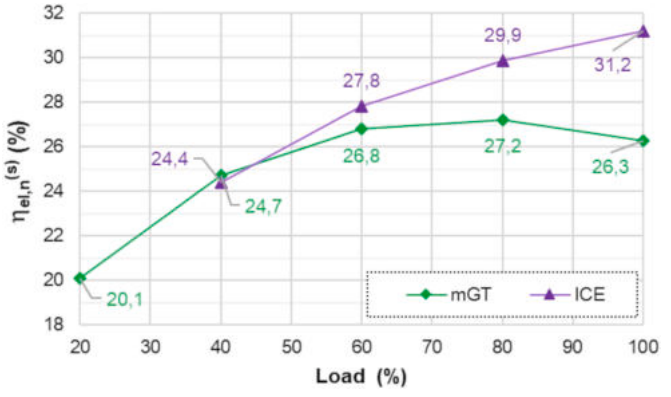


**Fig. 15.** Part load generator efficiency ($\eta_{el,n}^{(s)}$): ICE vs. mGT.

### 3.3. Scenarios of load-following mode: ICE vs. mGT

Daily patterns of electricity load were defined for a typical summer (Fig. 17a) and winter day (Fig. 17b). The peak power results to be 190 kW in summer and 168 kW in winter. The former implied that mGT accepts up to 112% of the rated load, within the limit on the generator output. It can be seen that there is a big variation in the power demand between day and night, within about 40% of the maximum load. Profiles of ambient temperature ($T_{amb}$), assumed as intake air temperature for ICE and mGT, are also shown in Fig. 17: $T_{amb}$ ranges from 17 to 35 °C in summer and from 2 to about 16 °C in winter. For each hour of day, the model was instructed to deliver a $P_{el,n}$ corresponding to the electricity demand, within the tolerance of 0.001%, by adjusting the load of ICE/mGT. To this end, use was made of the "control loop" algorithm available in Thermoflex®, which handles an iterative process with $P_{el,n}$ as the control set point. It should be pointed out that dynamics of the electromechanical system of the mTG was not incorporated in the model. However, the reader is remembered that, along with active power controller and speed controller, an additional voltage controller would be required in load-following operation to meet the power requirement while keeping both the terminal voltage and the frequency within their prescribed limits, as suggested by Shankar and Mukherjee (2014). Therefore, high quality power can be expected from the mTG in terms of frequency and voltage deviations during transient processes, even when fuel flexibility is tested (Piedrahita et al., 2021).

The first thing to point out is the different impact of $T_{amb}$ on the prime mover performance: it is relatively insignificant in the case of ICE, thanks to the turbocharger, and instead remarkable in the case of mGT. In the latter, in order to obtain the same power as $T_{amb}$ rises, the shaft speed must be increased to compensate for the reduced air density. Therefore, the compressor works at higher $\beta_C$ and corrected flow, thus providing a larger mass flow rate at a higher pressure (Caresana et al., 2014).

For better understanding, mGT operating points characterized by the same electricity load (of 168 kW) but different $T_{amb}$ were represented visually in the compressor map (Fig. 18). At the lowest $T_{amb}$ of 9.9 °C, a corrected flow of 0.0486 kg-mol/s (inlet airflow of 1.42 kg/s) is coupled with a $\beta_C$ of 3.9; at the highest $T_{amb}$ of 33.9 °C, corrected flow and $\beta_C$ rise to 0.0553 kg-mol/s (inlet airflow of 1.55 kg/s) and 4.3, respectively. The consequences of this are particularly evident in the summer day, from h. 8 to 14 (Fig. 19a): mGT inlet airflow rises from 1.485 to 1.550 kg/s to meet a stable electricity load, as $T_{amb}$ increases from 20 to 34 °C. In

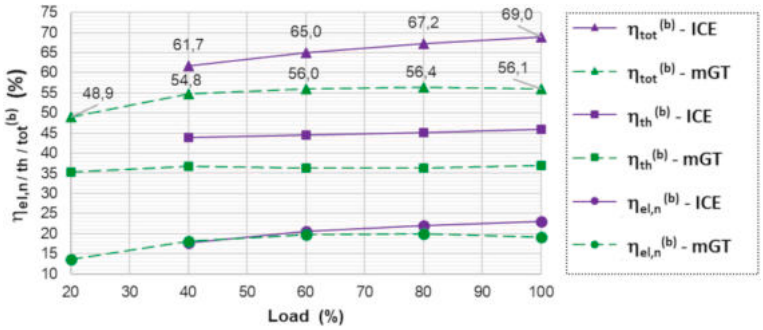


**Fig. 16.** Overall efficiency of the BtE chain at part load (ISO conditions): ICE vs. mGT.

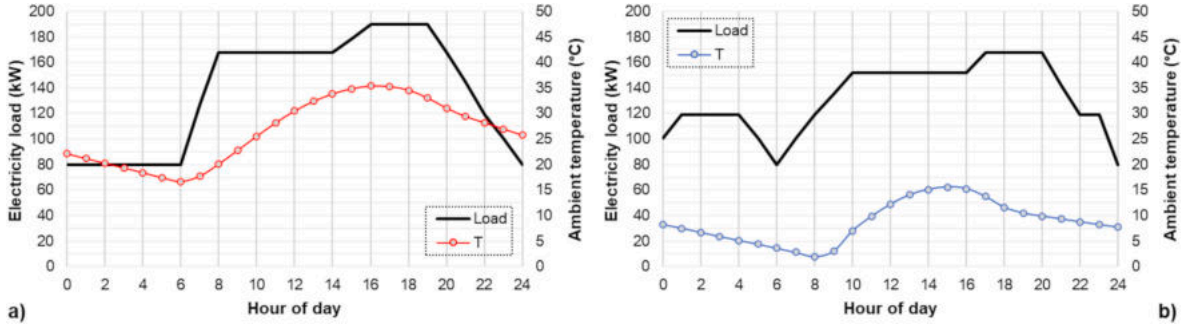


**Fig. 17.** Electricity load patterns and ambient temperature profiles in (a) summer and (b) winter day.

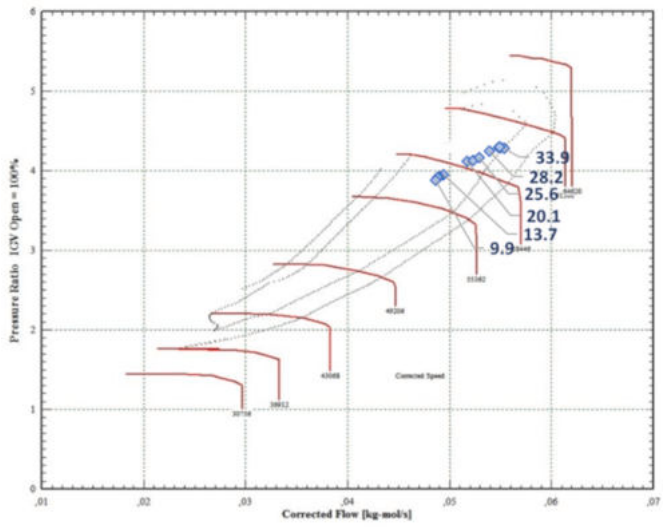


**Fig. 18.** Impact of ambient temperature (labels in °C) on mGT compressor operation at constant electricity load (168 kW).

contrast, the corresponding ICE intake air remains constant at 0.25 kg/s. However, for both prime movers, the inlet airflow increases with electrical demand, with the microturbine requiring far greater values than the ICE. The difference in syngas flow rate between ICE and mGT is minimal at low loads, i.e., at nighttime and during the winter day; conversely, the gap tends to widen at high loads, especially at high summer temperatures, when mGT requires more fuel than ICE (Fig. 19b).

The different off-design control strategies resulted in the electrical performance depicted in Fig. 20: $\eta^{(s)}_{el,g}$ (left) and $\eta^{(b)}_{el,n}$ (right) are placed side-by-side, for both summer (top) and winter (bottom) day. Starting from the left, at best, $\eta^{(s)}_{el,g}$ varies between 27.5% and 32% in summer day (Fig. 20a) and between 28.4% and 32.8% in winter day (Fig. 20c). The highest $\eta^{(s)}_{el,g}$ can be obtained with mGT over the entire winter day and during summer night. In the 10–20 time slot of the summer day, ICE is more efficient than mGT: the largest gain in $\eta^{(s)}_{el,g}$ of nearly 2.5 pp occurs at h. 15, when $T_{amb}$ is almost at its maximum, thus confirming that mGT is negatively affected by hot climate.

Paying attention to the graphs on the right, ICE emerges as the best solution. However, in summer day (Fig. 20b), a marginal difference between ICE and mGT curves occurs at nighttime, with the former ensuring a gain in $\eta^{(b)}_{el,n}$ within 1 pp and values of $\eta^{(b)}_{el,n}$ around 18–19%. The advantage of using ICE becomes more significant from h. 8 to 21: the largest discrepancy in $\eta^{(b)}_{el,n}$ reaches 6.2 pp at h. 15 due to the combination of high electricity load and warm $T_{amb}$. From h. 16 to 19, when the peak load is required by the grid at $T_{amb}$ ranging from 33 to 35 °C, $\eta^{(b)}_{el,n}$ for mGT remains around 17%, with a penalty of about 6 pp compared to ICE. As a result, mGT consumes much more biomass than ICE, over the whole day: 4.6 t. vs. 3.9 t, for a total electricity generation of 3330 kWh.

During the winter day, mGT lost its primacy in respect to ICE because of the change in the performance indicator, from $\eta^{(s)}_{el,g}$ of Fig. 20c to $\eta^{(b)}_{el,n}$ of Fig. 20d. In fact, it is substantially equivalent to ICE during nighttime hours, with $\eta^{(b)}_{el,n}$ falling in the range of 18.5%–20.7%, but less efficient in daytime. Nevertheless, the gap to ICE is smaller than during the summer day: at worst, 2.4 pp difference in $\eta^{(b)}_{el,n}$ occurs at h. 17. The reason for this is the burden of the FC, which becomes heavier as $\beta_C$ rises. Therefore, mGT case, when evaluated on the basis of $\eta^{(b)}_{el,n}$, may (slightly) outperform ICE when low loads combine with cold $T_{amb}$, as is the case from h. 5 to 7. Again, biomass consumption differs but only slightly: 3.8 t for ICE vs. 4.0 for mGT, to produce 3217 kWh.

Thermal performance is displayed in Fig. 21 for summer (top) and winter (bottom) day. Outputs from mGT are shown on the left for easy comparison with those from ICE, on the right. As for the summer day, during the central hours (from h. 10 to 20), mGT (Fig. 21a) yields more recoverable heat than ICE (Fig. 21b), with peak values of 455 $kW_{th}$ compared to 379 $kW_{th}$. This is mainly due to a much higher exhaust gas flow rate, whose discharge temperature increases with electricity load and $T_{amb}$, up to 327 °C. The opposite occurs in the remaining hours of the day, when mGT exhaust temperature falls by more than 60 °C below the

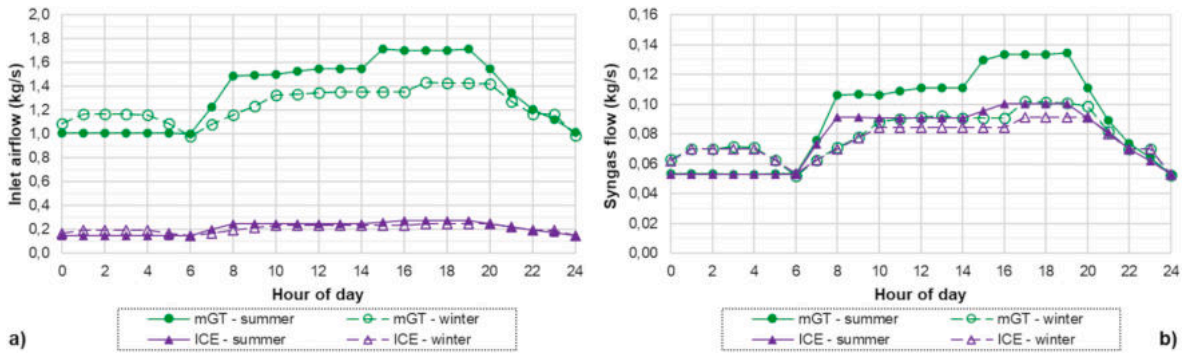


**Fig. 19.** Inlet airflow (a) and syngas flow rate (b) in summer and winter day: ICE vs. mGT.

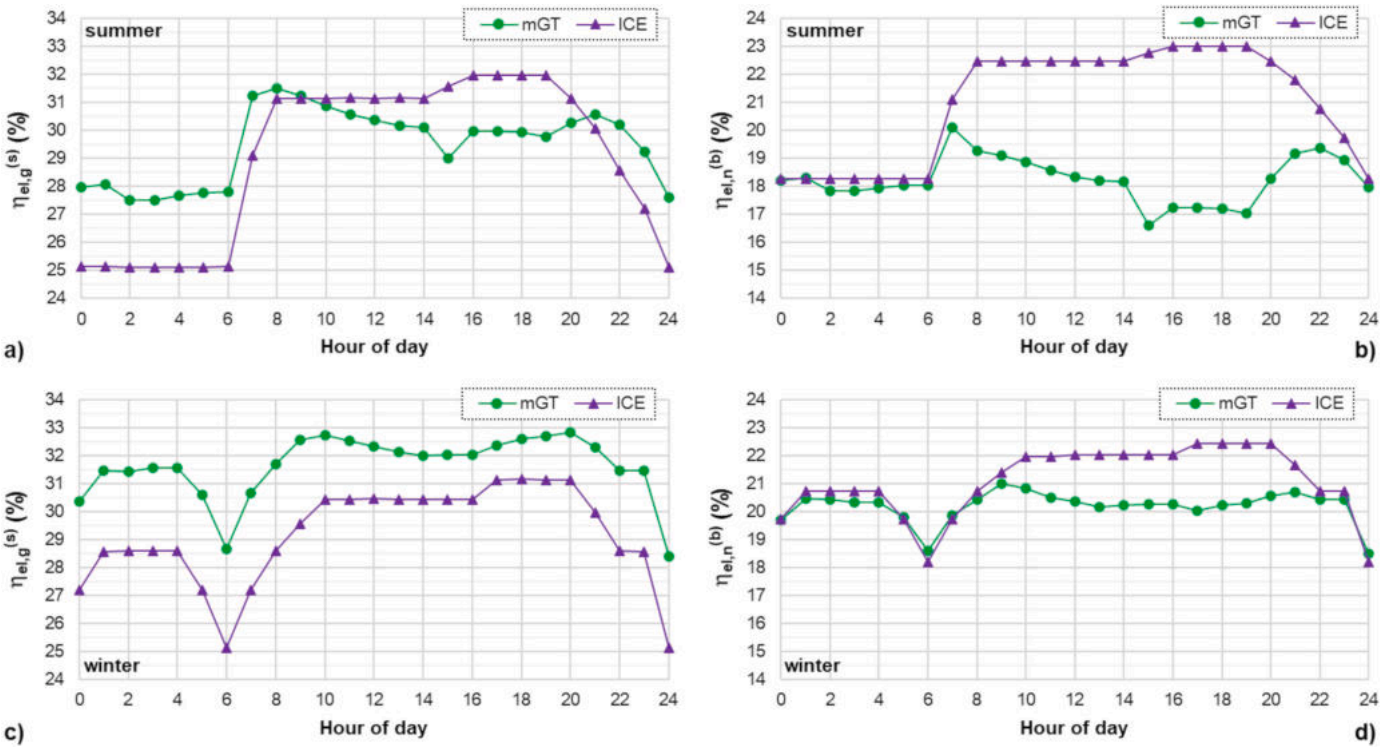


**Fig. 20.** BtE chain electrical performance, in terms of generator efficiency (left) and overall net electrical efficiency (right), in summer (top) and winter (bottom) day: ICE vs. mGT.

constant level of 344 °C set for ICE. Although the daily balance of recovered heat is in favor of the microturbine (7259 vs. 6991 $kWh_{th}$), ICE offers superior $\eta_{th}^{(b)}$ at any time of the day: values in the range of 44–46% are always higher than those of mGT (37–42%).

In the winter day, ICE is better than mGT in both aspects, namely heat recoverable and $\eta_{th}^{(b)}$. The former is larger at every hour of the day with a maximum of 340 $kW_{th}$ vs. 303 $kW_{th}$ for mGT. In addition, ICE maintains about the same $\eta_{th}^{(b)}$ levels as the summer day (44–46%) whereas mGT, being severely affected by the lowering of flue gas temperature below 263 °C, has a modest $\eta_{th}^{(b)}$ of 33–37%. The analyzed scenarios confirmed the key role of exhaust gas and HT circuit among the heat sources for mGT and ICE, respectively, whose total heat recovery is 5564 and 6774 $kWh_{th}$, on a daily basis.

Fig. 22 is devoted to $\eta_{tot}^{(b)}$ to assess CHP performance: it is clearly higher for ICE on any given day and time: the largest gap of 12 pp (68 vs 56%) occurs at h. 19 on the winter day while the smallest gap of about 5 pp (62 vs 57%) takes place at h. 24 on the summer day. Assuming one opts for ICE, the maximum $\eta_{tot}^{(b)}$ reaches 69% and its range is 62–69%, when both days are considered. In fact, corresponding values for mGT are 10 pp lower.

Finally, the daily quantity of $CO_2$ returned to the atmosphere was estimated by assuming complete oxidation of the hydrocarbon content of the syngas fuel. The data show that mGT is responsible for producing the largest amount of $CO_2$, whatever the day (Table 11). With reference to the 3rd and 4th columns, the difference in favor of ICE is small in winter but more significant in summer, due to the off-design adjustment of airflow and syngas flow rate explained in Section 3.3. As a matter of fact, the exhaust gas flow rate discharged by mGT is high enough to offset the much lower molar concentration of $CO_2$ at the stack, which was found to vary between 2 and 3.4% with load, compared with an almost constant value of 12.5%, in the case of ICE. To complete the emission picture, the residual sulfur content in the syngas stream was assumed to be oxidized to $SO_2$, resulting in the data collected in Table 12. Again, ICE is better than mGT, especially in the summer day.

It is clarified that the emission rates for stoichiometric compounds, such as $CO_2$ and $SO_2$, were computed directly from the simulation code. Conversely, the traces of non-stoichiometric pollutant compounds, such as $NO_x$, CO and unburned hydrocarbons, were not predicted by the model. They cannot be derived from first principles, as they are highly dependent on fuel properties, peak flame temperatures, mixing rates,

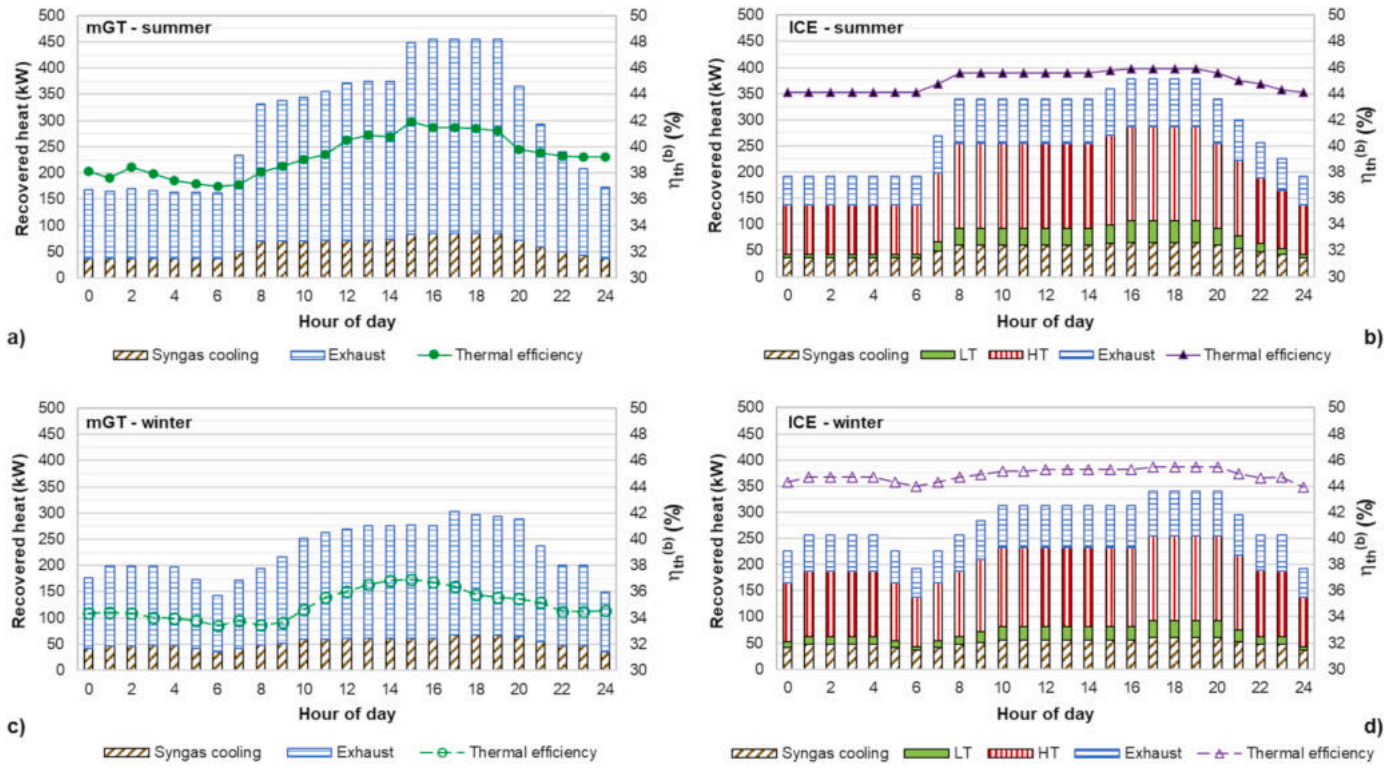


**Fig. 21.** BtE chain thermal performance, in terms of heat recovery and overall thermal efficiency ($\eta_{th}^{(b)}$), in summer (top) and winter (bottom) day: ICE (right) vs. mGT (left).

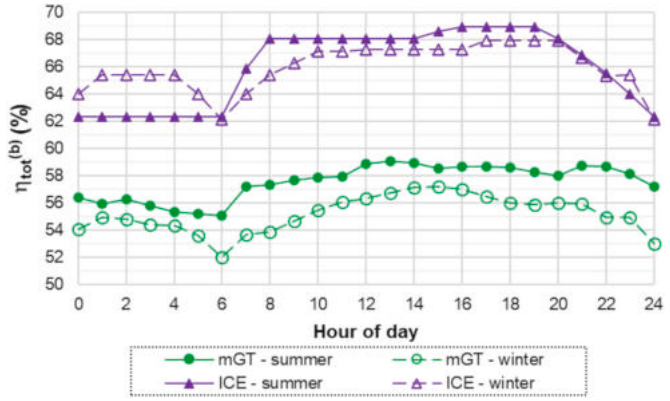


**Fig. 22.** BtE chain total efficiency, in summer and winter day: ICE vs. mGT.

**Table 11**
$CO_2$ emissions of BtE chain, in summer and winter day: ICE vs. mGT.

| Day | Parameter | BtE chain – ICE | BtE chain – mGT |
|---|---|---|---|
| Summer | kg/day | 4787 | 5654 |
| Winter | kg/day | 4666 | 4899 |

**Table 12**
$SO_2$ emissions of BtE chain, in summer and winter day: ICE vs. mGT.

| Day | Parameter | BtE chain – ICE | BtE chain – mGT |
|---|---|---|---|
| Summer | kg/day | 0.668 | 0.789 |
| Winter | kg/day | 0.651 | 0.684 |

and residence time within the combustion zone.

## 4. Conclusions

Energy performance of biomass gasification for small scale, CHP applications was evaluated for a target net power output of 200 $kW_{el}$. The BtE process was designed and modelled in a dual mode, with ICE or mGT as the prime mover, fed by syngas obtained from gasification of woody bamboo, after cold cleaning.

Assuming that ICE has the same nominal capacity as mGT (~240 $kW_{el}$), with NG as fuel, the power derating amounted to about 17% and 7%, respectively, when using syngas. However, ICE provided higher values of net electric power (190 vs. 179 kW) and overall net electrical efficiency (23.0 vs. 19.2%) than mGT when the BtE process is operated at full load and ISO conditions. The same applies to thermal efficiency, then to total efficiency.

Turning to partial load conditions, ICE confirmed to outperform mGT in terms of thermal and total efficiency, whatever the load. Regarding electricity generation, a distinction should be made based on the load level: at loads above 50%, ICE still provides the highest overall net electrical efficiency, with values between 19% and 23%; at low loads (50%–20%), mGT is slightly better than ICE, due to the reduction in the power absorbed by FC.

The lesson learnt from the load following mode of operation on two typical cold and hot days is that ICE is the most resilient system to the effects of ambient temperature on electrical and thermal performance. In contrast, atmospheric conditions have a deep influence on mGT behavior: warm weather can significantly lower the overall net electrical efficiency while boosting the total amount of recovered heat, albeit with still lower thermal efficiency than ICE. On both days, ICE met the demand from the grid with the lowest biomass consumption. Therefore, if the priority is given to power generation and recovered heat is considered a secondary output, ICE is better than mGT, unless the power plant operates at loads below 70%, in cold climates (at ambient temperature

below 10 °C).

However, when the generator is evaluated in terms of gross power divided by the energy input from syngas, mGT was found to achieve higher part load performance than ICE, except in hot weather. Under this condition, the lower density of the inlet air combines with higher energy consumption by the fuel compressor, so that the target power demand is met with lower net electric efficiency than in the case with ICE.

## 5. Future work

Further development of this study could address the "ecological efficiency" of the BtE chain to assess the thermoelectric performance with respect to pollutant emissions, as suggested by Boloy et al. (2011). Economic aspects also deserve attention, with the aim of providing the financial viability of a potential investment project throughout its lifetime (Copa et al., 2020). A conservative estimate of installation costs of approximately 4000 €/kW is a starting point, considering the wide range of 2000–6000 €/kW documented in the published literature (Quintero et al. (2021); Susanto et al. (2018)). The most influential economic model parameters should be the biomass cost, the sale price of electricity and the syngas yield (Colantoni et al., 2021).

Moreover, the analysis can be extended to other types of biomass, as the sustainability of the proposed power plant is inextricably linked to the availability of local resources. Finally, an organic Rankine cycle could be designed to provide an additional source of electricity by recovering waste heat from ICE and mGT.

## CRediT author statement

Mariaconcetta Fatiguso and Alessandro R. Valenti: Methodology, Software, Formal analysis, Validation. Silvia Ravelli: Conceptualization, Methodology, Writing - Original Draft, Writing - Review & Editing, Supervision.

## Funding

This research did not receive any specific grant from funding agencies in the public, commercial, or not-for-profit sectors.

## Declaration of competing interest

The authors declare that they have no known competing financial interests or personal relationships that could have appeared to influence the work reported in this paper.

## Data availability

The authors do not have permission to share data.

## Appendix A. Supplementary data

Supplementary data to this article can be found online at https://doi.org/10.1016/j.jclepro.2023.139782.

## APPENDIX A

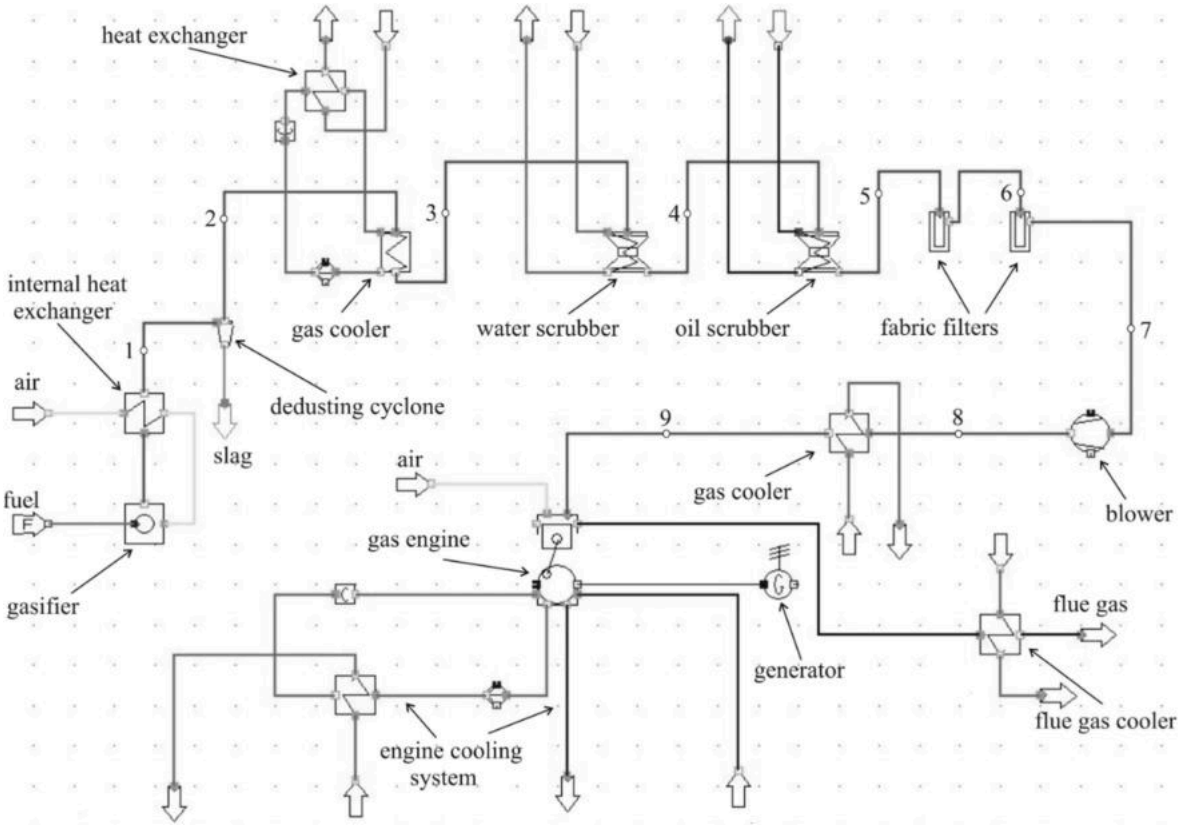


**Fig. A.1.** CHP installation based on biomass gasification taken from Elsner et al. (2017).

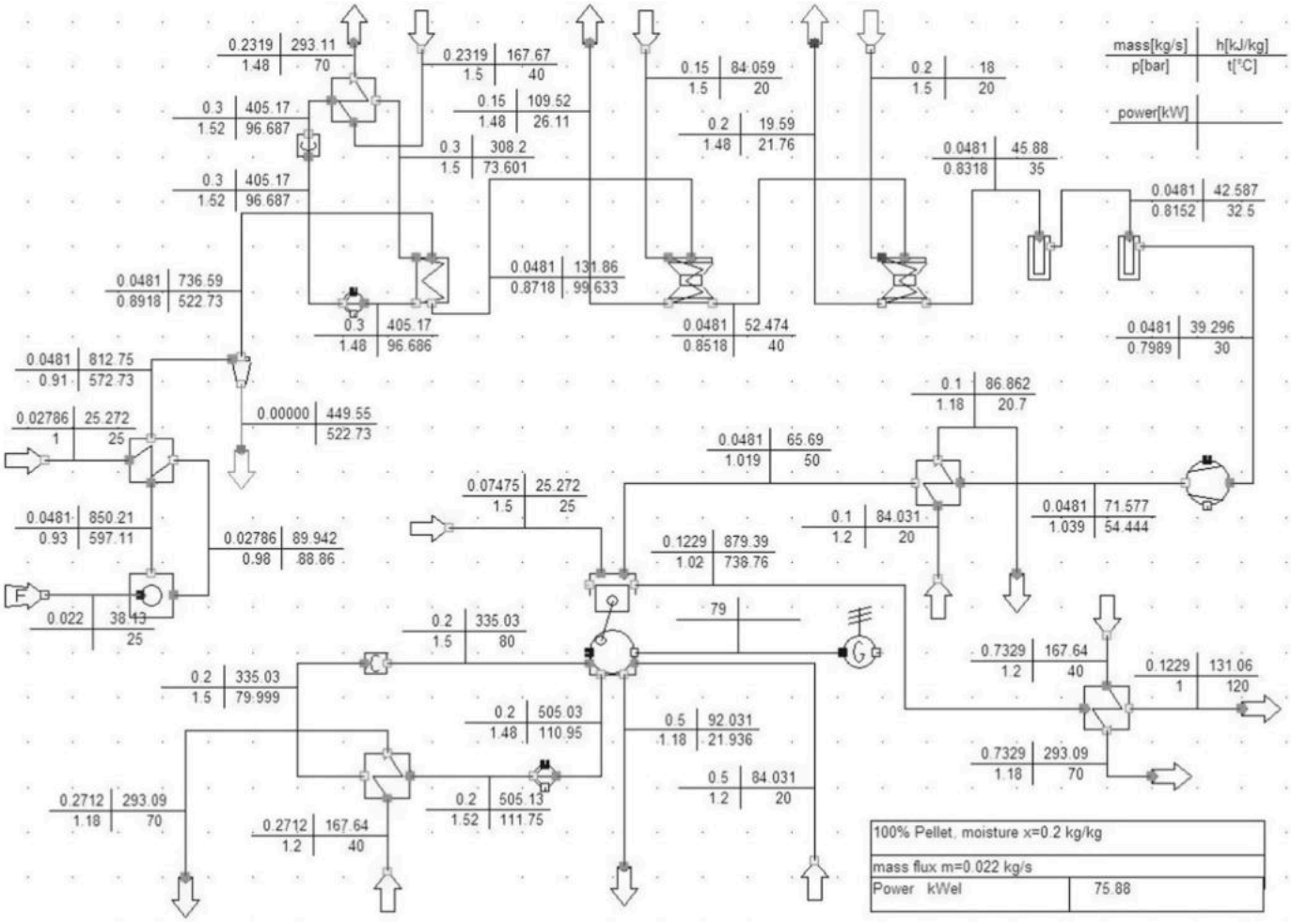


**Fig. A.2.** Sample configuration of the CHP installation proposed by Elsner et al. (2017).

## APPENDIX B

**Table B.1**
Operating conditions related to gas/air/fuel stream numbers in Fig. 2.

| Gas/Air | p | T | m | h | Mole Composition (%) | | | | | |
|---|---|---|---|---|---|---|---|---|---|---|
| Number | (bar) | (°C) | (kg/s) | (kJ/kg) | $N_2$ | $O_2$ | $CO_2$ | $H_2O$ | Ar | $SO_2$ |
| 4 | 1 | 100,2 | 0,0541 | 75,97 | 78,01 | 20,93 | 0,0303 | 0,0841 | 0,9396 | 0 |
| 6 | 1,02 | 15,68 | 0,0541 | −9397 | 78,01 | 20,93 | 0,0303 | 0,0841 | 0,9396 | 0 |
| 21 | 1013 | 15 | 0,2769 | −10,09 | 78,01 | 20,93 | 0,0303 | 0,0841 | 0,9396 | 0 |
| 22 | 1,02 | 344 | 0,3778 | 350,3 | 68,58 | 5456 | 12,43 | 12,72 | 0,8159 | 0,00119 |
| 34 | 1 | 120 | 0,3778 | 101,5 | 68,58 | 5456 | 12,43 | 12,72 | 0,8159 | 0,00119 |
| 43 | 1,02 | 15,68 | 0,0541 | −9397 | 78,01 | 20,93 | 0,0303 | 0,0841 | 0,9396 | 0 |
| 44 | 1013 | 15 | 0,0541 | −10,09 | 78,01 | 20,93 | 0,0303 | 0,0841 | 0,9396 | 0 |

| Fuel | p | T | m | h | Atomic Composition (%) | | | | | | LHV |
|---|---|---|---|---|---|---|---|---|---|---|---|
| Number | (bar) | (°C) | (kg/s) | (kJ/kg) | C | H | O | N | S | Ar | (kJ/kg) |
| 1 | 1013 | 15 | 0,0574 | 14,362 | 24,9 | 51,26 | 23,8 | 0,0375 | 0,0094 | 0 | 14,381 |
| 2 | 1 | 600 | 0,1065 | 6702 | 14,59 | 35,34 | 23,5 | 26,41 | 0,0065 | 0,1589 | 5845 |
| 3 | 1013 | 100 | 0,00502 | 22,372 | 100 | 0 | 0 | 0 | 0 | 0 | 22,310 |
| 7 | 0,9116 | 572,7 | 0,1065 | 6659 | 14,59 | 35,34 | 23,5 | 26,41 | 0,0065 | 0,1589 | 5845 |
| 8 | 1013 | 522,5 | 1,03E-07 | 6579 | 14,59 | 35,34 | 23,5 | 26,41 | 0,0065 | 0,1589 | 5845 |
| 9 | 0,8938 | 522,5 | 0,1065 | 6579 | 14,59 | 35,34 | 23,5 | 26,41 | 0,0065 | 0,1589 | 5845 |
| 10 | 0,8762 | 99,64 | 0,1065 | 5948 | 14,59 | 35,34 | 23,5 | 26,41 | 0,0065 | 0,1589 | 5845 |
| 13 | 0,8345 | 40,58 | 0,1063 | 5878 | 14,63 | 35,25 | 23,47 | 26,49 | 0,0065 | 0,1593 | 5857 |
| 16 | 0,8345 | 40,68 | 0,1063 | 5878 | 14,63 | 35,25 | 23,47 | 26,49 | 0,0065 | 0,1593 | 5857 |
| 17 | 1013 | 43,86 | 1,04E-07 | 5878 | 14,63 | 35,25 | 23,47 | 26,49 | 0,0065 | 0,1593 | 5857 |
| 18 | 0,7948 | 19,97 | 0,1009 | 6159 | 15,92 | 32,48 | 22,6 | 28,82 | 0,0015 | 0,1607 | 6165 |
| 23 | 0,9299 | 600 | 0,1065 | 6702 | 14,59 | 35,34 | 23,5 | 26,41 | 0,0065 | 0,1589 | 5845 |

(continued on next page)

**Table B.1** (*continued*)

| Fuel | p | T | m | h | Atomic Composition (%) | | | | | | LHV |
|---|---|---|---|---|---|---|---|---|---|---|---|
| Number | (bar) | (°C) | (kg/s) | (kJ/kg) | C | H | O | N | S | Ar | (kJ/kg) |
| 31 | 1033 | 40,25 | 0,1009 | 6186 | 15,92 | 32,48 | 22,6 | 28,82 | 0,0015 | 0,1607 | 6165 |
| 45 | 0,7948 | 19,97 | 0,1051 | 5814 | 14,89 | 34,69 | 23,3 | 26,96 | 0,0014 | 0,1622 | 5919 |
| 46 | 1014 | 20 | 0,00117 | −2173,8 | 0 | 66,67 | 33,04 | 0 | 0,2908 | 0 | 248,9 |

**Table B.2**
Operating conditions related to gas/air/fuel stream numbers in Fig. 3.

| Gas/Air | p | T | m | h | Mole Composition (%) | | | | | |
|---|---|---|---|---|---|---|---|---|---|---|
| Number | (bar) | (°C) | (kg/s) | (kJ/kg) | $N_2$ | $O_2$ | $CO_2$ | $H_2O$ | Ar | $SO_2$ |
| 4 | 1 | 100,2 | 0,061 | 75,97 | 78,01 | 20,93 | 0,0303 | 0,0841 | 0,9396 | 0 |
| 6 | 1,02 | 15,68 | 0,061 | −9397 | 78,01 | 20,93 | 0,0303 | 0,0841 | 0,9396 | 0 |
| 20 | 1 | 120 | 1674 | 97,44 | 75,57 | 16,99 | 3174 | 3355 | 0,9076 | 3,02E-04 |
| 21 | 1013 | 275,2 | 1674 | 259,7 | 75,57 | 16,99 | 3174 | 3355 | 0,9076 | 3,02E-04 |
| 22 | 4397 | 191,2 | 1,56 | 168,5 | 77,96 | 20,92 | 0,0303 | 0,1562 | 0,9389 | 0 |
| 25 | 4341 | 531,3 | 1,56 | 529,7 | 77,96 | 20,92 | 0,0303 | 0,1562 | 0,9389 | 0 |
| 31 | 4256 | 863,7 | 1674 | 927,2 | 75,57 | 16,99 | 3174 | 3355 | 0,9076 | 3,02E-04 |
| 32 | 1044 | 581 | 1674 | 596,3 | 75,57 | 16,99 | 3174 | 3355 | 0,9076 | 3,02E-04 |
| 33 | 1013 | 15 | 1,56 | −10,09 | 77,96 | 20,92 | 0,0303 | 0,1562 | 0,9389 | 0 |
| 43 | 1,02 | 15,68 | 0,061 | −9397 | 78,01 | 20,93 | 0,0303 | 0,0841 | 0,9396 | 0 |
| 44 | 1013 | 15 | 0,061 | −10,09 | 78,01 | 20,93 | 0,0303 | 0,0841 | 0,9396 | 0 |

| Fuel | p | T | m | h | Atomic Composition (%) | | | | | | LHV |
|---|---|---|---|---|---|---|---|---|---|---|---|
| Number | (bar) | (°C) | (kg/s) | (kJ/kg) | C | H | O | N | S | Ar | (kJ/kg) |
| 1 | 1013 | 15 | 0,0646 | 14,362 | 24,9 | 51,26 | 23,8 | 0,0375 | 0,0094 | 0 | 14,381 |
| 2 | 1 | 600 | 0,1199 | 6702 | 14,59 | 35,34 | 23,5 | 26,41 | 0,00648 | 0,1589 | 5845 |
| 3 | 1013 | 100 | 0,00565 | 22,372 | 100 | 0 | 0 | 0 | 0 | 0 | 22,310 |
| 7 | 0,9117 | 572,7 | 0,1199 | 6658 | 14,59 | 35,34 | 23,5 | 26,41 | 0,00648 | 0,1589 | 5845 |
| 8 | 1013 | 522,5 | 1,03E-07 | 6578 | 14,59 | 35,34 | 23,5 | 26,41 | 0,00648 | 0,1589 | 5845 |
| 9 | 0,8939 | 522,5 | 0,1199 | 6578 | 14,59 | 35,34 | 23,5 | 26,41 | 0,00648 | 0,1589 | 5845 |
| 10 | 0,8763 | 99,65 | 0,1199 | 5948 | 14,59 | 35,34 | 23,5 | 26,41 | 0,00648 | 0,1589 | 5845 |
| 13 | 0,8346 | 40,58 | 0,1197 | 5878 | 14,63 | 35,25 | 23,47 | 26,49 | 0,0065 | 0,1593 | 5857 |
| 16 | 0,8346 | 40,73 | 0,1197 | 5878 | 14,63 | 35,25 | 23,47 | 26,49 | 0,0065 | 0,1593 | 5857 |
| 17 | 1013 | 43,86 | 1,04E−07 | 5878 | 14,63 | 35,25 | 23,47 | 26,49 | 0,0065 | 0,1593 | 5857 |
| 18 | 0,7949 | 20 | 0,1137 | 6159 | 15,92 | 32,48 | 22,6 | 28,82 | 0,00153 | 0,1607 | 6165 |
| 19 | 4341 | 185,2 | 0,1137 | 6384 | 15,92 | 32,48 | 22,6 | 28,82 | 0,00153 | 0,1607 | 6165 |
| 23 | 0,93 | 600 | 0,1199 | 6702 | 14,59 | 35,34 | 23,5 | 26,41 | 0,00648 | 0,1589 | 5845 |
| 45 | 0,7949 | 20 | 0,1184 | 5814 | 14,89 | 34,69 | 23,3 | 26,96 | 0,00143 | 0,1622 | 5919 |
| 46 | 1014 | 20,03 | 0,00132 | −2173,7 | 0 | 66,67 | 33,04 | 0 | 0,2908 | 0 | 249 |

## APPENDIX C

For compressor and turbine, respectively, the relationship between pressure ratio ($\beta_C$, $\beta_T$) vs. corrected flow (CF–FF), with lines for each value of corrected speed (CS), was implemented by applying the following definitions:

$$CF = \frac{m_a \sqrt{\frac{T_{in,C}}{T_{ref}}}}{MW \frac{p_{in,C}}{p_{ref}}} \tag{10}$$

$$FF = \frac{C\, m_{exh}}{p_{in,T}} \sqrt{\frac{\left(\frac{R}{MW \gamma_{exh}}\right) T_{in,T}}{\left(\frac{2}{\gamma_{exh}+1}\right)^{\frac{\gamma_{exh}+1}{\gamma_{exh}-1}}}} \tag{11}$$

$$CS = n \sqrt{\frac{T_{ref}}{T_{in}}} \tag{12}$$

with $T_{ref} = 288.15$ K and $p_{ref} = 1.013$ bar. In Eq. (11), universal gas constant (R), molecular weight (MW) and specific heat ratio ($\gamma$) reflect changes in exhaust composition when syngas replaces NG.

On each CS line, 10 points were defined with values of pressure ratio, corrected flow, and polytropic efficiency normalized with respect of design conditions, as follows:

$$\frac{CF}{(CF)_{Design\ Point}} \tag{13}$$

$$\frac{FF}{(FF)_{Design\ Point}} \tag{14}$$

$$\frac{CS}{(CS)_{Design\ Point}} \tag{15}$$

$$\frac{\beta}{(\beta)_{Design\ Point}} \tag{16}$$

$$\frac{\eta_y}{\eta_y - (\eta_y)_{Design\ Point}} \tag{17}$$

Values of $CF, FF, CS, \beta_C, \beta_T, \eta_y$ at design point derive from the thermodynamic parameters reported in Section 2.3.2 at full load, ISO conditions, with NG as fuel. Consequently, nominal CF in compressor map is 0.0549 kg-mol/s whereas nominal CS is 60,000 rpm. For the turbine, nominal FF equals 0.0034 $m^2$ whereas nominal CS is 29,074 rpm.

## References


Article 29. Sustainability and greenhouse gas emissions saving criteria for biofuels, bioliquids and biomass fuels. Directive (EU) 2018/2001. https://lexparency.org/eu/32018L2001/ART_29/.

Bates, R.P., Dölle, K., 2017. Syngas use in internal combustion engines-a review. Adv. Res. 10 (1), AIR.32896, 1–8.

Bocci, E., Sisinni, M., Moneti, M., et al., 2014. State of art of small scale biomass gasification power systems: a review of the different typologies. Energy Proc. 45, 247–256. https://doi.org/10.1016/j.egypro.2014.01.027.

Boloy, R.A.M., Silveira, J.L., Tuna, C.E., et al., 2011. Ecological impacts from syngas burning in internal combustion engine: technical and economic aspects. Renew. Sustain. Energy Rev. 15 (9), 5194–5201. https://doi.org/10.1016/j.rser.2011.04.009.

Bonasio, V., Ravelli, S., 2022. Performance analysis of an ammonia-fueled micro gas turbine. Energies 15 (11), 3874. https://doi.org/10.3390/en15113874.

Briones-Hidrovo, A., Copa, J., Tarelho, L.A., et al., 2021. Environmental and energy performance of residual forest biomass for electricity generation: gasification vs. combustion. J. Clean. Prod. 289, 125680 https://doi.org/10.1016/j.jclepro.2020.125680.

Caligiuri, C., Žvar Baškovič, U., Renzi, M., et al., 2021. Complementing syngas with natural gas in spark ignition engines for power production: effects on emissions and combustion. Energies 14 (12), 3688. https://doi.org/10.3390/en14123688.

Capstone, 2009. Capstone C200 Microturbine Technical Reference, 410066. Rev C.

Caresana, F., Pelagalli, L., Comodi, G., et al., 2014. Microturbogas cogeneration systems for distributed generation: effects of ambient temperature on global performance and components' behavior. Appl. Energy 124, 17–27. https://doi.org/10.1016/j.apenergy.2014.02.075.

Chang, C.T., Costa, M., La Villetta, M., et al., 2019. Thermo-economic analyses of a Taiwanese combined CHP system fuelled with syngas from rice husk gasification. Energy 167, 766–780. https://doi.org/10.1016/j.energy.2018.11.012.

Colantoni, A., Villarini, M., Monarca, D., Carlini, M., et al., 2021. Economic analysis and risk assessment of biomass gasification CHP systems of different sizes through Monte Carlo simulation. Energy Rep. 7, 1954–1961. https://doi.org/10.1016/j.egyr.2021.03.028.

Copa, J.R., Tuna, C.E., Silveira, J.L., et al., 2020. Techno-economic assessment of the use of syngas generated from biomass to feed an internal combustion engine. Energies 13 (12), 3097. https://doi.org/10.3390/en13123097.

Corrêa Jr., P.S.P., Zhang, J., Lora, E.E.S., et al., 2019. Experimental study on applying biomass-derived syngas in a microturbine. Appl. Therm. Eng. 146, 328–337. https://doi.org/10.1016/j.applthermaleng.2018.09.123.

Dasappa, S., Subbukrishna, D.N., Suresh, K.C., et al., 2011. Operational experience on a grid connected 100 kWe biomass gasification power plant in Karnataka, India. Energy Sustain. Dev. 15 (3), 231–239. https://doi.org/10.1016/j.esd.2011.03.004.

Elsner, W., Wysocki, M., Niegodajew, P., et al., 2017. Experimental and economic study of small-scale CHP installation equipped with downdraft gasifier and internal combustion engine. Appl. Energy 202, 213–227. https://doi.org/10.1016/j.apenergy.2017.05.148.

Fiore, M., Magi, V., Viggiano, A., 2020. Internal combustion engines powered by syngas: a review. Appl. Energy 276, 115415. https://doi.org/10.1016/j.apenergy.2020.115415.

Gabbrielli, R., Seggiani, M., Frigo, S., et al., 2016. Validation of a small scale woody biomass downdraft gasification plant coupled with gas engine. Chem. Eng. Trans. 50, 241–246. https://doi.org/10.3303/CET1650041.

Gobbato, P., Masi, M., Benetti, M., 2015. Performance analysis of a producer gas-fuelled heavy-duty SI engine at full-load operation. Energy Proc. 82, 149–155. https://doi.org/10.1016/j.egypro.2015.12.007.

Hadi Jafari, P., Kowsary, F., 2014. Thermoeconomic comparison between the performance of small-scale internal combustion engines and gas turbines integrated with a biomass gasifier. Energy Equip. Syst. 2 (1), 57–82.

Hagos, F.Y., Aziz, A.R.A., Sulaiman, S.A., 2014. Trends of syngas as a fuel in internal combustion engines. Adv. Mech. Eng. 6, 401587 https://doi.org/10.1155/2014/401587.

Hamad, M.A.F., Radwan, A.M., Amin, A., 2017. Review of biomass thermal gasification. In: Biomass Volume Estimation and Valorization for Energy. IntechOpen. https://doi.org/10.5772/66362.

Hampel, C.A., Braun, R.J., 2022. Off-design modeling of a microturbine combined heat & power system. Appl. Therm. Eng. 202, 117670 https://doi.org/10.1016/j.applthermaleng.2021.117670.

Havilah, P.R., Sharma, A.K., Govindasamy, G., et al., 2022. Biomass gasification in downdraft gasifiers: a technical review on production, up-gradation and application of synthesis gas. Energies 15 (11), 3938. https://doi.org/10.3390/en15113938.

IEA, 2022. Bioenergy, Paris. https://www.iea.org/reports/bioenergy. License: CC BY 4.0.

Indrawan, N., Kumar, A., Moliere, M., et al., 2020. Distributed power generation via gasification of biomass and municipal solid waste: a review. J. Energy Inst. 93 (6), 2293–2313. https://doi.org/10.1016/j.joei.2020.07.001.

Kirubakaran, V., Sivaramakrishnan, V., Nalini, R., Sekar, T., et al., 2009a. Studies on auto-gasification of bio-residues. Energy Sources, Part A 31 (11), 967–973. https://doi.org/10.1080/15567030801904541.

Kirubakaran, V., Sivaramakrishnan, V., Nalini, R., Sekar, T., et al., 2009b. A review on gasification of biomass. Renew. Sustain. Energy Rev. 13 (1), 179–186. https://doi.org/10.1016/j.rser.2007.07.001.

Koido, K., Iwasaki, T., 2018. Biomass Gasification: A Review of its Technology, Gas Cleaning Applications, and Total System Life Cycle Analysis. InTech. https://doi.org/10.5772/intechopen.70727.

La Villetta, M., Costa, M., Cirillo, D., et al., 2018. Performance analysis of a biomass powered micro-cogeneration system based on gasification and syngas conversion in a reciprocating engine. Energy Convers. Manag. 175, 33–48. https://doi.org/10.1016/j.enconman.2018.08.017.

Le Coq, L., Ashenafi, D., 2012. Syngas treatment unit for small scale gasification-application to IC engine gas quality requirement. J. Appl. Fluid Mech. 5 (1), 95–103.

Lee, M.C., Seo, S.B., Chung, J.H., et al., 2010. Gas turbine combustion performance test of hydrogen and carbon monoxide synthetic gas. Fuel 89 (7), 1485–1491. https://doi.org/10.1016/j.fuel.2009.10.004.

Lee, U., Balu, E., Chung, J.N., 2013. An experimental evaluation of an integrated biomass gasification and power generation system for distributed power applications. Appl. Energy 101, 699–708. https://doi.org/10.1016/j.apenergy.2012.07.036.

Liu, A., Weng, Y., 2009. Effects of lower heat value fuel on the operations of micro-gas turbine. Energy Power Eng. 1 (1), 28–37. https://doi.org/10.4236/epe.2009.11005.

Mărculescu, C., Cenuşă, V.E., Alexe, F.N., 2016. Analysis on using biomass lean syngas in micro gas turbines. IOP Conf. Ser. Earth Environ. Sci. 40 (1), 012036 https://doi.org/10.1088/1755-1315/40/1/012036.

Moretti, L., Arpino, F., Cortellessa, G., Di Fraia, S., et al., 2021. Reliability of equilibrium gasification models for selected biomass types and compositions: an overview. Energies 15 (1), 61. https://doi.org/10.3390/en15010061.

Mustafi, N.N., Miraglia, Y.C., Raine, R.R., et al., 2006. Spark-ignition engine performance with 'Powergas' fuel (mixture of $CO/H_2$): a comparison with gasoline and natural gas. Fuel 85 (12–13), 1605–1612. https://doi.org/10.1016/j.fuel.2006.02.017.

Nicolosi, F.F., Renzi, M., 2018. Effect of the regenerator efficiency on the performance of a micro gas turbine fed with alternative fuels. Energy Proc. 148, 687–694. https://doi.org/10.1016/j.egypro.2018.08.158.

Olivieri, A., Ravelli, S., 2020. Cogasification of coal and biomass in an integrated gasification combined cycle power plant: effects on thermodynamic performance and gas composition. J. Energy Eng. 146 (6), 04020071 https://doi.org/10.1061/(ASCE)EY.1943-7897.0000716.

Othman, N.F., Boosroh, M.H., 2016. Effect of $H_2$ and CO contents in syngas during combustion using Micro Gas Turbine. IOP Conf. Ser. Earth Environ. Sci. 32 (1), 012037 https://doi.org/10.1088/1755-1315/32/1/012037.

Pathak, B.S., Kapatel, D.V., Bhoi, P.R., et al., 2007. Design and development of sand bed filter for upgrading producer gas to IC engine quality fuel. Int. Energy J. 8 (1), 15–20.

Patuzzi, F., Basso, D., Vakalis, S., et al., 2021. State-of-the-art of small-scale biomass gasification systems: an extensive and unique monitoring review. Energy 223, 120039. https://doi.org/10.1016/j.energy.2021.120039.

Piedrahita, C.A.R., Acosta, R.A., Sánchez, Y.A.C., 2021. Performance of a capstone gas turbine based power plant working on high Butane LPG. South Florida J. Dev. 2 (5),

7977–7990. https://www.southfloridapublishing.com/ojs/index.php/jdev/article/download/987/843.
Pradhan, A., Baredar, P., Kumar, A., 2015. Syngas as an alternative fuel used in internal combustion engines: a review. J. Pure Appl. Sci. Technol. 5 (2), 51–66. ISSN: 2249-9970 (Online).
Quintero, J.S.G., Gonzalez, C.A.D., Sandoval, L.P., 2021. Exergoeconomic analysis of a simulated system of biomass gasification-based power generation with surplus syngas storage in a rural zone in Colombia. Sustain. Energy Technol. Assessments 44, 101075. https://doi.org/10.1016/j.seta.2021.101075.
Rabou, L.P., Grift, J.M., Conradie, R.E., Fransen, S., 2008. Micro gas turbine operation with biomass producer gas and mixtures of biomass producer gas and natural gas. Energy Fuels 22 (3), 1944–1948.
Raman, P., Ram, N.K., 2013. Performance analysis of an internal combustion engine operated on producer gas, in comparison with the performance of the natural gas and diesel engines. Energy 63, 317–333. https://doi.org/10.1016/j.energy.2013.10.033.
Ravelli, S., 2021. Part-load operation of gas turbines induced by Co-gasification of coal and biomass in an integrated gasification combined cycle power plant. In: Turbo Expo: Power for Land, Sea, and Air, vol. 84997. ASME, V006T03A011. https://doi.org/10.1115/GT2021-59830.
Renzi, M., Patuzzi, F., Baratieri, M., 2017. Syngas feed of micro gas turbines with steam injection: effects on performance, combustion and pollutants formation. Appl. Energy 206, 697–707. https://doi.org/10.1016/j.apenergy.2017.08.214.
Salovaara, J., Romero-Tehuitzil, H., Vaca, M.C.M., et al., 2015. Pre-operational analysis of a prototype downdraft gasifier fueled by bamboo. J. Sustain. Bioenergy Syst. 5 (2), 62. https://doi.org/10.4236/jsbs.2015.52006.
Schipfer, F., 2019. Sustainable and optimal use of biomass for energy in the EU beyond 2020. German Federal Ministry of Agriculture, EU. http://task40.ieabioenergy.com/roles-of-bioenergy-technologies-in-energy-system-pathways-towards-a-wb2-sdg-world/.RolesofbioenergytechnologiesinenergysystempathwaystowardsaWB2/SDGworld. http://hdl.handle.net/20.500.12708/76804.
Shankar, G., Mukherjee, V., 2014. Load-following performance analysis of a microturbine for islanded and grid connected operation. Int. J. Electr. Power Energy Syst. 55, 704–713. https://doi.org/10.1016/j.ijepes.2013.10.018.
Siemens Energy, Inc., 2017a. SGE-S Series Gas Engines and Gen-Sets Natural Gas - 1,200/1,500/1,800 Rpm. Article-No.PGDR-B10015-00-4AUS.
Siemens Energy, Inc., 2017b. Siemens Gas Engines Fuel Flexibility – Power Ratings. Article-No. PGDR-B10014-00-4AUS.
Situmorang, Y.A., Zhao, Z., Yoshida, A., et al., 2020. Small-scale biomass gasification systems for power generation (<200 kW class): a review. Renew. Sustain. Energy Rev. 117, 109486 https://doi.org/10.1016/j.rser.2019.109486.
Squilbin, O., Gerlagh, T., Barreto, L., et al., 2020. Biomass Mobilisation and Sustainability, CA-RES3 Report. https://www.ca-res.eu/fileadmin/cares/PublicArea/CA-RES3FinalPublication/CARES3_Final_CT4_Summary.pdf.
Sridhar, G., Sridhar, H.V., Dasappa, S., et al., 2005. Development of producer gas engines. Proc. Inst. Mech. Eng., Part D: J. Automobile Eng. 219 (3), 423–438. https://doi.org/10.1243/095440705X6596.
Susanto, H., Suria, T., Pranolo, S.H., 2018. Economic analysis of biomass gasification for generating electricity in rural areas in Indonesia. IOP Conf. Ser. Mater. Sci. Eng. 334 (1), 012012 https://doi.org/10.1088/1757-899X/334/1/012012.
Susastriawan, A.A.P., Saptoadi, H., 2017. Small-scale downdraft gasifiers for biomass gasification: a review. Renew. Sustain. Energy Rev. 76, 989–1003. https://doi.org/10.1016/j.rser.2017.03.112.
Thermoflex®, 2023, Volume 3, Fully-flexible Heat Balance Calculation, Chapter 5, section 5.9.4.2 Multi-Parameter Scaling, © Copyright Thermoflow, Inc., 1987-2023, Jacksonville, FL, US..
Thomson, R., Kwong, P., Ahmad, E., et al., 2020. Clean syngas from small commercial biomass gasifiers; a review of gasifier development, recent advances and performance evaluation. Int. J. Hydrogen Energy 45 (41), 21087–21111. https://doi.org/10.1016/j.ijhydene.2020.05.160.
Uma, R., Kandpal, T.C., Kishore, V.V.N., 2004. Emission characteristics of an electricity generation system in diesel alone and dual fuel modes. Biomass Bioenergy 27 (2), 195–203. https://doi.org/10.1016/j.biombioe.2004.01.003.
Vargas-Salgado, C., Águila-León, J., Alfonso-Solar, D., et al., 2022. Simulations and experimental study to compare the behavior of a genset running on gasoline or syngas for small scale power generation. Energy 244, 122633. https://doi.org/10.1016/j.energy.2021.122633.
Wi, S.G., Lee, D.S., Nguyen, Q.A., et al., 2017. Evaluation of biomass quality in short-rotation bamboo (Phyllostachys pubescens) for bioenergy products. Biotechnol. Biofuels 10, 127. https://doi.org/10.1186/s13068-017-0818-9.
Woolcock, P.J., Brown, R.C., 2013. A review of cleaning technologies for biomass-derived syngas. Biomass Bioenergy 52, 54–84. https://doi.org/10.1016/j.biombioe.2013.02.036.